



# Oxidation Behavior of Hf-Modified Aluminide Coatings on Inconel-718 at 1050°C

Yongqing Wang<sup>a,†,\*</sup>, James L. Smialek<sup>b</sup> and Marc Suneson<sup>a,†</sup>

<sup>a</sup>SIFCO Minneapolis, Turbine Component Services, 2430 North Winnetka Avenue, Minneapolis, MN, 55427, USA

<sup>b</sup>NASA Glenn Research Center, Cleveland, OH 44135, USA

**Abstract:** Simple  $\beta$ -NiAl, Hf-modified  $\beta$ -NiAl, Pt-diffused, Pt-modified  $\beta$ -(Ni,Pt)Al +  $\xi$ -PtAl<sub>2</sub>, and Hf-Pt-modified  $\beta$ -(Ni,Pt)Al were cyclic oxidation tested at 1050°C in air on Inconel-718 substrates for up to 4370h. The Pt-diffused specimen failed most quickly, < 100 h, while the simple  $\beta$ -NiAl aluminide maintained a positive weight change for ~1300 h. The Pt-modified aluminides clearly improved the cyclic oxidation behavior of both simple and Hf-modified aluminides, sustaining a zero weight change only after 3600 and 4000 h, respectively. The Hf additions did not immediately appear to produce as strong an improvement as expected, however, they were more highly ranked when normalized by coating thickness. They also decreased surface rumpling, important for TBC durability. Hf-rich NiAl grain boundaries, formed during coating processing, resulted in HfO<sub>2</sub> particles in the scales and oxide pegs at the metal interface, all suggesting some level of over-doping. The high sulfur content of the substrate influenced spalling to bare metal and re-healing to less protective Ni(Al,Cr)<sub>2</sub>O<sub>4</sub> spinel-type and (Ti,Cr,Nb)O<sub>2</sub> rutile scales. The evolution of these surface features have been documented over 100 to 4370 h of exposure. The coating aluminum content near failure was ~2-3 wt. %.

Received on 07-03-2014  
 Accepted on 10-04-2014  
 Published on 25-06-2014

**Keywords:** Hafnium, aluminide coatings, oxidation testing, Inconel 718, vapor phase process.

DOI: <http://dx.doi.org/10.6000/2369-3355.2014.01.01.4>

## 1. INTRODUCTION

Diffusion aluminide coatings, as either environmental coatings or as bond coats in thermal barrier coating (TBC) systems, have been widely applied on turbine engine hot section blades and vane segments as protection from the aggressive conditions of industrial and aero-gas turbines. This protection derives from the promotion of a slow growing Al<sub>2</sub>O<sub>3</sub> oxide scale that acts as a barrier against oxidation and hot corrosion. Ideally, the alumina scale should be slow-growing, adherent, compact, and continuous to be effective under cyclic, high temperature, corrosive engine environments [1]. Excessive scale spallation from the bond coat leads to TBC failure, and excessive scale growth contributes to scale spallation [2, 3].

The performance of aluminide coatings has been improved to meet the requirements of increasing turbine operating temperatures by doping the aluminide coatings with other elements. Pt-doped aluminide coatings, produced by

electroplating a thin layer of Pt followed by aluminizing, have increased coating lifetimes significantly [4-9]. Currently, the single phase  $\beta$ -(Ni,Pt)Al coating has been an accepted industrial standard as the bond coat for TBCs [10]. However, the cost of Pt-modified aluminide coatings is higher due to the extra electroplating step as well as the price of Pt. The role of Pt is complex and has been shown to counteract sulfur segregation, enable alumina formation at lower Al content, and maintain a higher Al surface concentration [11-15]. Nevertheless, continued growth of an alumina scale and interdiffusion with the substrate result in Al depletion in the  $\beta$ -NiAl coatings and transformation from  $\beta$ -NiAl to  $\gamma$ '-Ni<sub>3</sub>Al during cycling [16, 17]. The associated volume change, coupled with CTE mismatch with superalloy substrates, results in coating surface "rumpling" that accelerates delamination of the ceramic top coat when used in a TBC system [18, 19]. As a result, there is a desire to incorporate other elements either to replace Pt in aluminide coatings or to further improve the performance of Pt-modified aluminide coatings. Hf doping is one approach of growing interest. The benefits of Hf are well documented in previous studies of various Hf-doped cast alloys, such as Co-10Cr-11Al (wt. %)+Hf [20-23], Ni-10Cr-8Al (wt. %)+Hf [24], NiAl+Hf [25-31],  $\gamma$ -Ni/ $\gamma$ '-Ni<sub>3</sub>Al+Hf [32], FeCrAl+Hf [33, 34], as well as plasma sprayed NiCoCrAlHfY coatings [35]. The various mechanisms

\*SIFCO Minneapolis, Turbine Component Services, 2430 North Winnetka Avenue, Minneapolis, MN, 55427, USA; Tel: 1-336-969-1246; Fax: 1-336-969-1539; E-mails: yongqingblessing@gmail.com, yongqing.wang@siemens.com

<sup>†</sup>Current Address: Siemens Energy, Inc. at 3050 Westinghouse Road, Rural Hall, NC, 27045 and. Marc Suneson is at Mohawk Metallurgical Associates.

by which performance is enhanced by Hf and other reactive elements have been studied in detail, as summarized in review papers [36-39].

Hf additions, in particular, markedly improve scale adherence and reduce the scale growth rate. Furthermore, it has recently been proposed that Hf additions may decrease the surface rumpling [40]. Accordingly, promising results from bulk alloys are being transferred to coating applications. It is well known that interdiffusion with various substrates may provide unintentional compositional changes and provide the primary mode of Al loss, both leading to oxidative degradation [41, 42]. Thus it is paramount to demonstrate acceptable performance for future applications by oxidation testing and characterization of actual Hf-doped aluminide coatings.

Regarding such diffusion coatings, Hf may be incorporated by interdiffusion from Hf-containing substrates [40, 43-44] or from the coating process environment [45]. For industrial applications, it is more practical and versatile to incorporate Hf from the coating process. However, co-deposition has been proven to be problematic [31, 46]. Thus much of what is known about Hf effects in  $\beta$ -NiAl had initially been gained from Hf-doped model cast alloys or where the Hf-doping was accomplished by substrate interdiffusion or pre-sputtered Hf [28, 47-48].

Many of the process fundamentals of co-deposited aluminides were first presented by Kim *et al.* [46], showing important  $\text{HfCl}_3/\text{AlCl}_3$  activator ratios producing various Hf concentrations and grain boundary segregation of Hf. Recently a commercial coating patent application (Howmet) described the use of an optimized Pt-electroplate and pre-hafnizing to  $\text{Hf}_2\text{Pt}_3\text{Ni}_x$   $\mu$ -phase compounds, followed by aluminizing [49]. The resultant Hf-Pt-NiAl bond coatings have been shown to be capable of a 3-5 $\times$  improvement in TBC life (i.e., ca. 3000-3500 cycles at 1135°C, 45 min./cycle for 7YSZ) [49].

Finally work at SIFCO [50, 51] showed that Hf could be successfully incorporated into aluminide coatings on Ni-base superalloys by using an industrial vapor phase coating process. The various process parameters studied previously for the base coating included Pt electroplate thickness, Al content in the source alloy, and diffusion heat treatments for Mar M-247, Inconel 625, and Waspalloy substrates [50]. In general, greater Al and Pt amounts led to greater amounts of the  $\xi$ -PtAl<sub>2</sub> phase, subsequently decreased by diffusion annealing. Hf-doped simple NiAl or Pt-doped NiAl coatings were then produced on six different alloys, including aero-engine hot section components. In general, extremely Hf-rich coating grain boundaries were identified along with Hf-rich particles dispersed throughout the thickness and enrichment at the coating interface, yielding a relatively inhomogeneous Hf distribution.

Despite a high level of interest in this and other such coating advancements, there is relatively little information available characterizing the details of their oxidation behavior,

especially for coatings produced by commercial processes. Indeed most Hf, Zr -doped coating oxidation studies have been for alternate processing routes, such as Hf pre-sputtering or EB-PVD NiAl(+Cr, Zr) [47, 52]. One doped aluminizing study found beneficial trends in 1150°C cyclic oxidation performance with the amount of  $\text{HfO}_2$  or  $\text{ZrO}_2$  pack sources, but such studies are rare [53].

Accordingly, the purpose of the present study was to characterize the cyclic oxidation behavior of some developmental Hf-doped aluminide coatings on a generic Ni-base superalloy, Inconel 718. It is recognized that low sulfur, oxidation resistant 2<sup>nd</sup> and 3<sup>rd</sup> generation single crystal alloys may be a more critical class of substrates. Their excellent performance with Ni(Pt)Al bond coats and TBCs enables their widespread use as turbine blades and vanes. However, Inconel 718 was chosen for this early developmental study as one of those previously studied during coating development and one which does not contain Hf that might obscure Hf effects from just the coating. Simple  $\beta$ -NiAl, Hf-modified  $\beta$ -NiAl, Pt-diffused, Pt-modified  $\beta$ -(Ni,Pt)Al +  $\xi$ -PtAl<sub>2</sub>, and Hf-Pt-modified  $\beta$ -(Ni,Pt)Al coatings were oxidized at 1050°C in air, using primarily 20 hr cycles. Unlike many cyclic oxidation studies of bulk or coated materials, periodic examinations provided insightful demonstration of the evolution of surface scale structures from initial oxidation, through the maximum in weight gain, to where the systems were steadily losing weight by spallation and finally exhibited a negative weight change. Such exposures went up to ~4400 h for the Hf-Pt-NiAl coating.

## 2. EXPERIMENTAL PROCEDURE

Specimens for this study were machined from conventional Inconel 718 sheet purchased from Haynes International with a certified composition of 53.52Ni-17.64Fe-18.61Cr-5.15Nb-3.02Mo-0.2Co-1.03Ti-0.51Al-0.05Si-0.22Mn-0.02Cu-0.03C-0.003S (wt. %). Five different coatings were tested: diffused Pt, NiAl, Hf-NiAl, Pt-NiAl, and Hf-Pt-NiAl. The specimen sizes were approximately 30 mm  $\times$  25 mm  $\times$  1.6 mm for the NiAl coating and 40mm  $\times$  30 mm  $\times$  1.6 mm for the others. All the Pt coatings were first electroplated with 4-7  $\mu\text{m}$  Pt and diffusion heat treated at 1052°C for 1h in vacuum [51]. All four aluminide coatings were produced at 1080°C for 3-4 h by a vapor phase coating process using Cr-Al alloy sources and  $\text{AlF}_3$  activator [51]. Hf-doped aluminides were produced with  $\text{HfO}_2$  powder added in the retort [50].

Specimens were ultrasonically cleaned in water and acetone, and then cyclically oxidized side by side in an F48020 Thermolyne, benchtop muffle furnace in air. In each cycle, specimens were manually loaded at a furnace temperature of 850°C, automatically ramped to 1050°C over 35 minutes, held at 1050°C for a specified time, generally 20 h per cycle. The samples were then cooled to 850°C in 20 minutes, unloaded manually, further cooled in ambient air, and weighed. Only the dwell time, the time length from the point

when the temperature reaches 1050°C to the point when the furnace starts to cool down, was counted as oxidation test time. The hot dwell was 5h/cycle for the first 40 h, 20h/cycle between 40h and 3320h, and 150h/cycle between 3320h and 4370 h. The testing condition in this research is a little bit different from the traditional cyclic oxidation testing condition in which the sample is directly loaded and unloaded at the test temperature. The sample weights were measured with a Scientech SA 80 balance to 0.1 mg, and the specific weight change was calculated using the entire sample surface area. The evolution of the surface scale morphology was tracked at various stages during oxidation testing. Both surface

morphology and the cross-section microstructures were examined after coating failure (~0.3 mg/cm<sup>2</sup> weight loss, i.e., just crossing zero weight change) using a JEOL scanning electron microscope (SEM) equipped with Oxford energy dispersive spectroscopy (EDS).

### 3. RESULTS

#### 3.1. Coating Characterization Prior to Oxidation Testing

The as-coated surface morphology and cross-section information were obtained from a duplicate specimen,

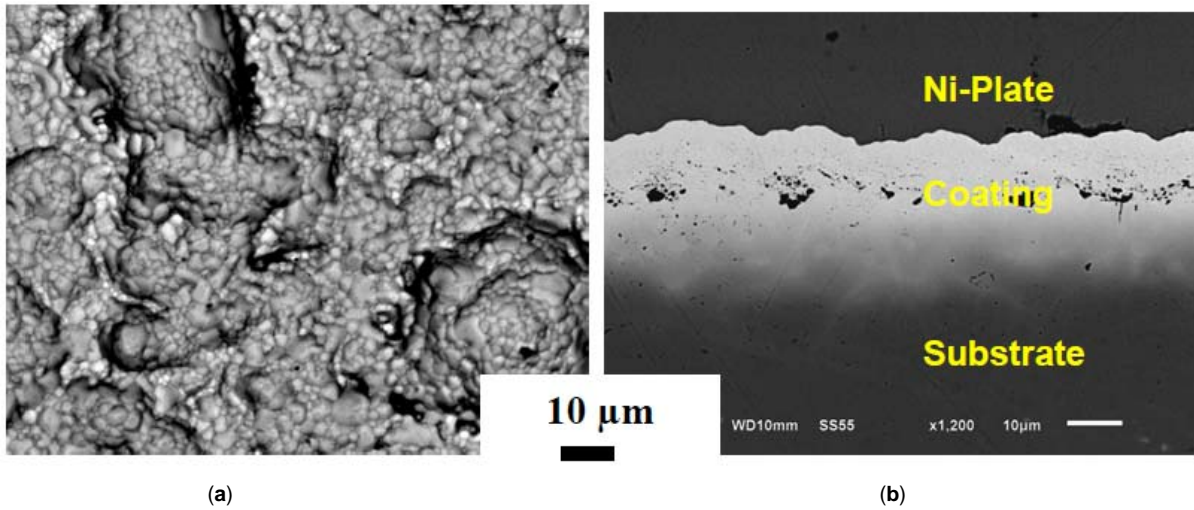


**Figure 1:** SEM backscattered electron micrographs of as-diffused Pt-coating. (a) Surface morphology, and (b) Cross-section.

**Table 1:** Summary of Estimated Coating Compositions on Inconel 718 before and after Cyclic Oxidation at 1050°C (wt. % by EDS, ~20 h/Cycle)

	Ni	Al	Cr	Fe	Ti	Nb	Mo	Pt
<b>IN-718</b>	<b>53.2</b>	<b>0.5</b>	<b>18.6</b>	<b>18.5</b>	<b>1</b>	<b>5.2</b>	<b>3</b>	
Pt diffused	21.1	0.7	9.2	8.5	1.1	3.9	2.2	52.7
100 h	43.4		8.5	17.6			4.1	26.4
<b>Δ wt %</b>	<b>22.3</b>	<b>-0.7</b>	<b>-0.7</b>	<b>9.1</b>	<b>-1.1</b>	<b>-3.9</b>	<b>1.9</b>	<b>-26.3</b>
Pure NiAl	48.6	34.8	5.3	11.2				
1500 h	72.9	8.2	3.3	6.6	2.2	6.9		
<b>Δ wt %</b>	<b>24.3</b>	<b>-26.6</b>	<b>-2.0</b>	<b>-4.6</b>	<b>2.2</b>	<b>6.9</b>	<b>0</b>	<b>0</b>
Hf-NiAl	45.2	32	7.5	15.3				
2000 h	55.1	2.6	16.5	17.1	1.1	5	2.6	
<b>Δ wt %</b>	<b>9.9</b>	<b>-29.4</b>	<b>9.0</b>	<b>1.8</b>	<b>1.1</b>	<b>5</b>	<b>2.6</b>	<b>0</b>
Pt-NiAl	42.4	18.8	4.9	5.5	0.4			28.5
4070 h	54.1	3.6	15.2	15.1	1.1	4.9		6
<b>Δ wt %</b>	<b>11.7</b>	<b>-15.2</b>	<b>10.3</b>	<b>9.6</b>	<b>0.7</b>	<b>4.9</b>	<b>0</b>	<b>-22.5</b>
Hf-Pt-NiAl	43.4	29.2	0.9	4.4				22.1
4370h	53.6	2.2	16.6	16.8	1.1	4.4		5.3
<b>Δ wt %</b>	<b>10.2</b>	<b>-27.0</b>	<b>15.7</b>	<b>12.4</b>	<b>1.1</b>	<b>4.4</b>	<b>0</b>	<b>-16.8</b>

MDC150L.

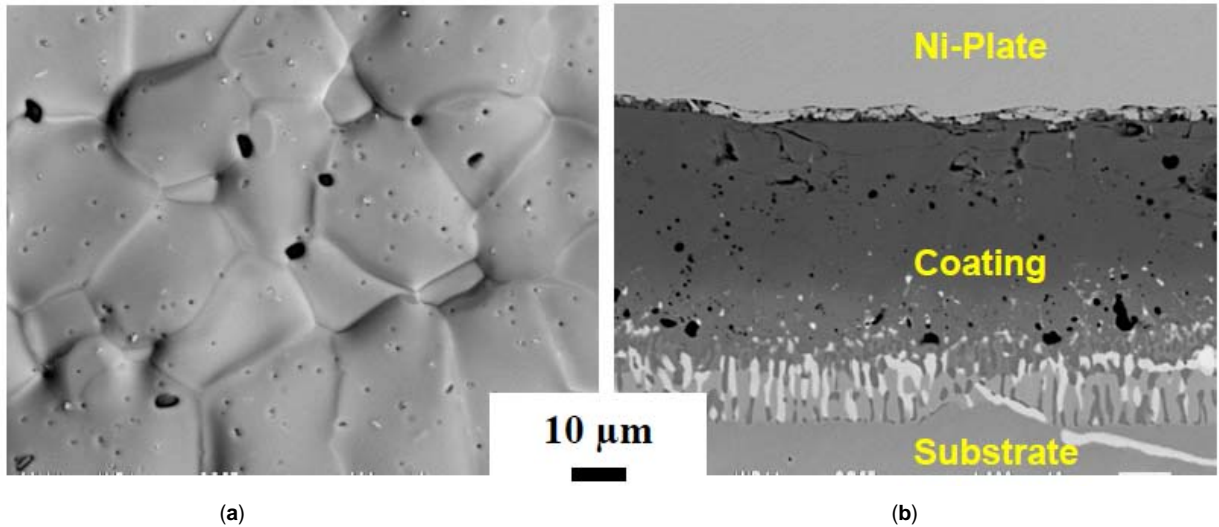


**Figure 2:** SEM backscattered electron micrographs of as-processed NiAl coating. (a) Surface morphology, and (b) Cross-section.

processed along with the oxidation specimens. Some details were published previously [50, 51], but major features are presented below:

#### Diffused Pt

After electroplating and vacuum diffusion annealing for 1 h at 1052°C, the Pt-coating surface shows a fine grain structure (Figure 1a). Coating EDS analysis, summarized in Table 1, indicated the surface was very Pt-rich with an estimated composition of (wt. %) 52.7Pt-21.1Ni-9.2Cr-8.5Fe-3.9Nb-0.7Al-1.1Ti-2.2Mo-0.6Co. The Pt-rich layer was observed to be around 30μm in cross-section (Figure 1b).

#### NiAl

The simple β-NiAl coatings were produced by the industrial vapor phase coating process. The as-coated surface showed the typical large, 25-50 μm polyhedral shaped grains (Figure 2a). The EDS surface composition was 48.6Ni-34.8Al-5.3Cr-

11.2Fe (wt. %), indicating Al-rich β-NiAl phase (Stoichiometric β-NiAl is ~31.5 wt. % Al). In cross-section (Figure 2b), the coating was measured to be 62 μm thick and composed of two layers: an outer β-NiAl phase additive layer and an interdiffusion layer.

#### Hf-NiAl

The Hf-doped NiAl coating was also produced by the industrial vapor phase coating process. The as-coated surface (Figure 3a) showed 10-20 μm polyhedral shaped grains with a composition of 45.2Ni-32.0Al-7.5Cr-15.3Fe (wt. %), indicating β-NiAl. The bright grain boundaries at the surface were rich in Hf. In cross-section (Figure 3b), the coating was measured to be 58 μm thick and exhibited bright Hf-rich precipitates near the coating surface and at the interface between the outer β-NiAl layer and the interdiffusion layer.

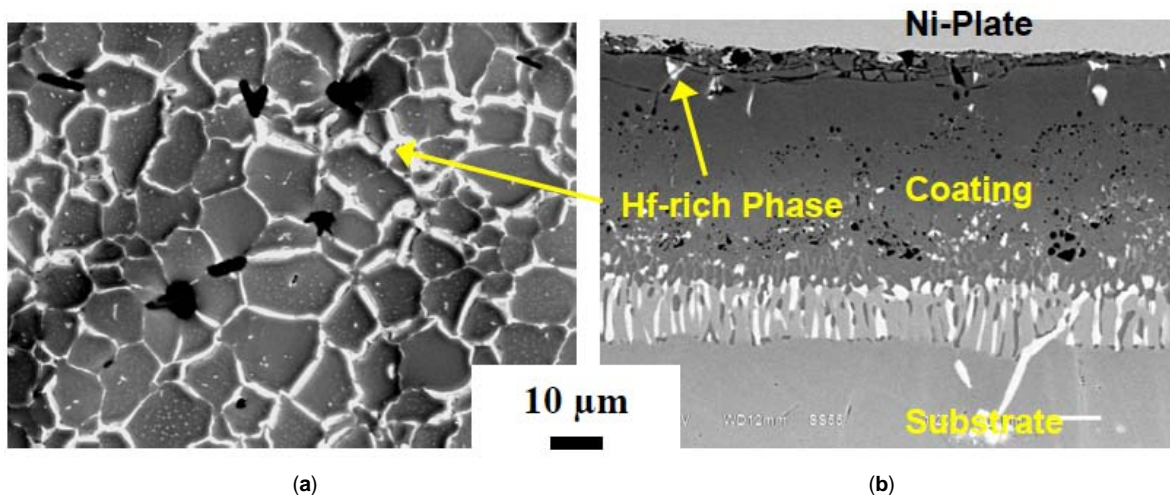


**Figure 3:** SEM backscattered electron micrographs of as-processed Hf-NiAl coating. (a) Surface morphology, and (b) Cross-section.

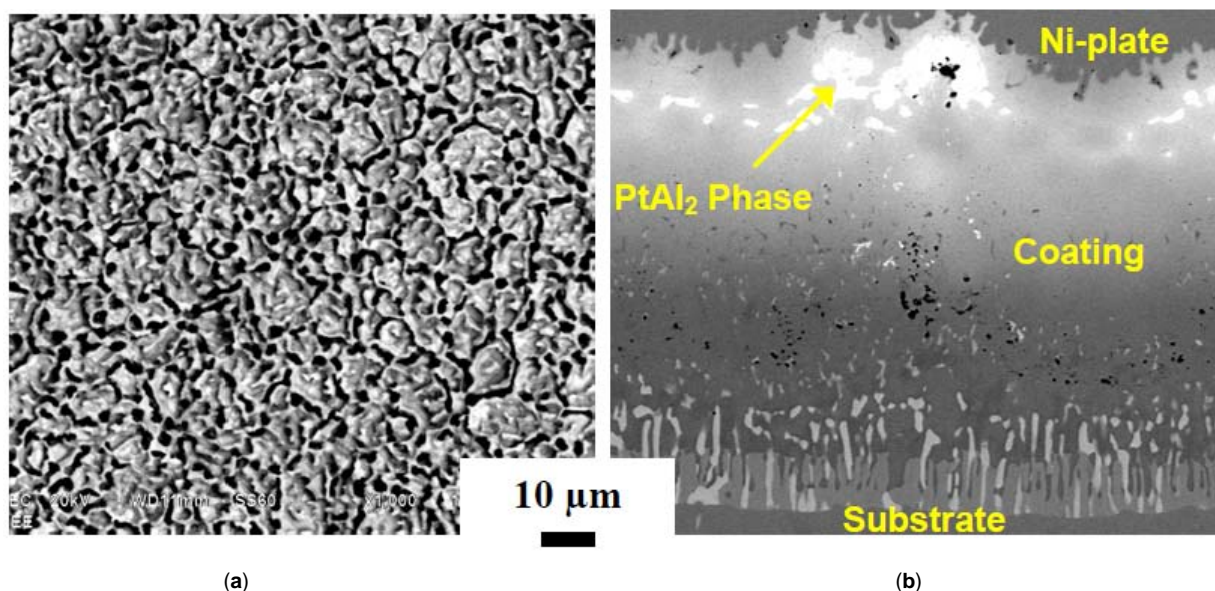


**Figure 4:** SEM backscattered electron micrographs of as-processed Pt-NiAl coating. (a) Surface morphology, and (b) Cross-section.

#### **Pt-NiAl**

The Pt-NiAl coating was synthesized *via* Pt electroplating, vapor phase aluminizing, and heat treating at 1121°C for 2h in vacuum. The coating surface (Figure 4a) was irregular, with a network of ~5 μm cusps and dimples. The surface composition was 42.4Ni 18.4Al-4.9Cr-5.5Fe-0.4Ti-28.5Pt (wt. %), suggesting a hypostoichiometric β-(Ni,Pt)Al phase in the 2-phase region with γ-Ni<sub>3</sub>Al. The irregular cusp-like surface is also visible in cross-section (Figure 4b). The coating was 101μm thick and consisted of two layers: an outer additive layer and an interdiffusion layer. Some bright ξ-PtAl<sub>2</sub> phase particles remained in the outer layer after the heat treatment.

#### **Hf-Pt-NiAl**

The Hf-Pt-doped NiAl coating was prepared *via* Pt electroplating, vapor phase co-aluminizing & hafnizing, and heat treating at 1121°C for 2h in vacuum. The coating also showed an irregular coating surface with ~5 μm cusps (Figure 5a), as did the other Pt-doped NiAl coating. The surface was composed of bright ridge areas (A) and gray areas (B) in Figure 5b. The bright ridge phase is Hf-Pt-rich with a composition of 20.8Hf-36.7Ni-18.3Al-0.7Cr-4.0Fe-1.1Co-18.5Pt (wt. %), while the gray phase is β-(Ni,Pt)Al with a composition of 43.4Ni-29.2Al-0.9Cr-4.4Fe-22.1Pt (wt.%). In cross-section (Figure 5c), the coating was measured to be 71 μm thick, again showing the irregular surface with the Hf-Pt-rich phases. Within the coating, fine bright Hf-rich particles were observed in the outer β-(Ni,Pt)Al layer.

It is known that ppm levels of sulfur (S) have a detrimental effect on alumina scale adhesion and cyclic oxidation resistance of aluminides and that Hf can be effective in restoring adhesion in the presence of sulfur [28, 54-55]. Consequently, the Hf and S depth profiles were determined by Glow-Discharge Mass Spectrometry (GDMS) and

compared for the NiAl and Hf-NiAl coatings in Figure 6. The S distribution in the NiAl coating was around 7 - 40 ppm in the outer layer and showed a peak value of 269 ppm at the interface between the outer and interdiffusion layers. Similarly, S in the Hf-NiAl coating was 7-50 ppm within the outer layer, and the peak value at the interface was 126 ppm. The Hf distribution in the NiAl coating was only 1 ppm within the outer layer and a peak value of 8 ppm at the interface with the interdiffusion layer. In contrast, Hf in the Hf-NiAl coating was 0.39 wt. % at the external coating surface and 0.05-0.11 wt. % within the outer additive layer.

The above comparison indicated that the S contents were comparable in both coatings and consistent with the 30 ppmw (0.003 wt. %) S content in the substrate; while Hf in the Hf-NiAl coating was substantially higher. Since the substrate did not contain any Hf and no Hf source material was used in the coating process for the simple NiAl coating, the minor Hf in that coating was expected to result from contamination. It can be ignored for oxidation effects because of the low levels. It should be mentioned that coating depth here was converted from sputtering time and a sputtering rate typical for GDMS analysis. Furthermore, significant uncertainty inherent in the GDMS techniques (possibly above 20%), due to non-uniform sputtering and phase inhomogeneity, may give rise to some systematic errors.

### **3.2. Cyclic Oxidation Weight Change**

A number of points are raised in showing and analyzing the weight change data below. Briefly, all coatings show an increase in weight due to oxidation, exhibit a maximum, and then weight loss due to spalling. This shift occurs latest for the Pt-NiAl and Pt-Hf-NiAl coatings. A parabolic plot of weight vs  $t^{1/2}$  indicates an initial transient for all coatings and a specified range to best fit parabolic behavior between ~20-

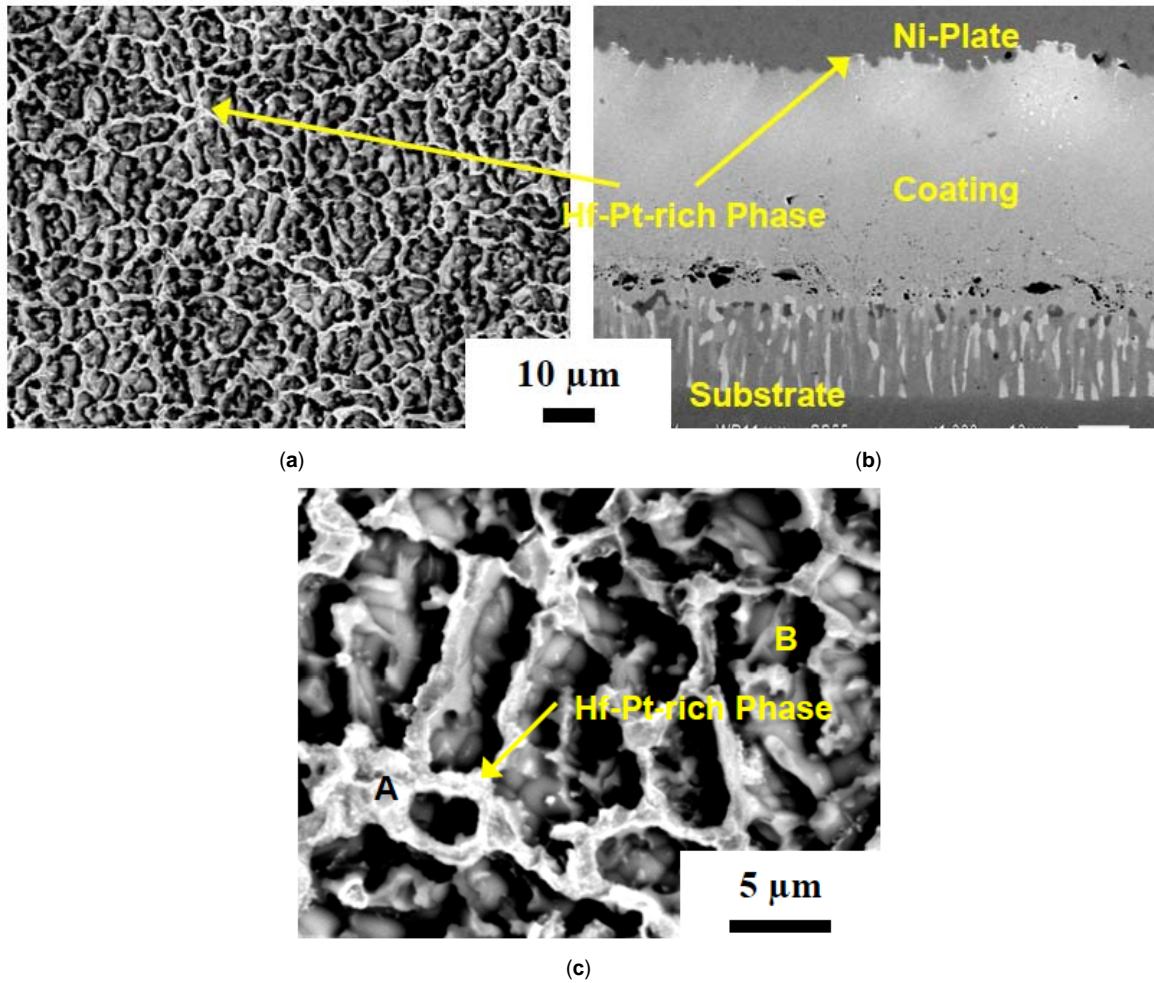


Figure 5: SEM backscattered electron micrographs of as-processed Hf-Pt-NiAl coating. (a) Surface morphology, (b) Cross-section, and (c) Hf-Pt-rich phase on coating surface.

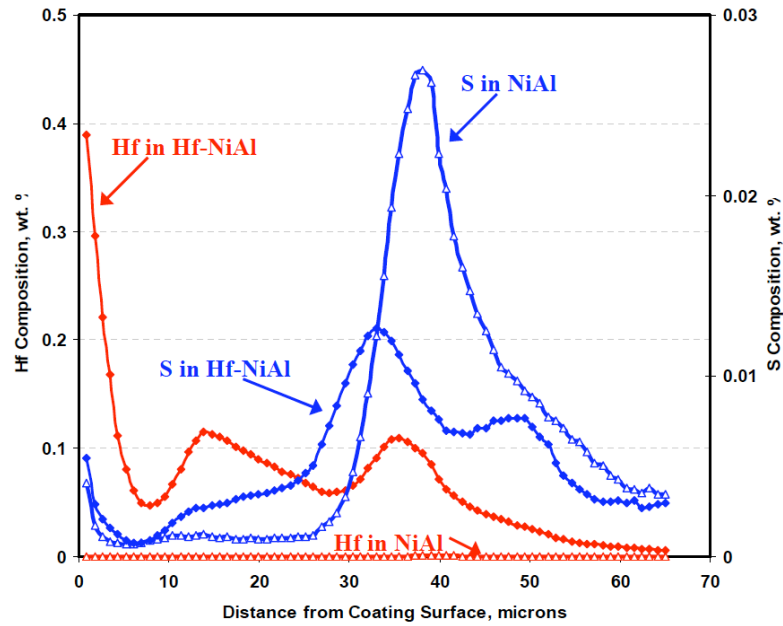


Figure 6: GDMS composition depth profiles of Hf and S in the NiAl and Hf-NiAl coatings.

**Table 2: Characteristic Cyclic Oxidation Parameters for Coatings on Inconel 718. (1050°C, ~20 h/cycle)  $t_0$ , Time to Crossover;  $t_{spall}$ , Time to Deviate from Parabolic;  $k_p$ , Estimated from Initial Portion of Curves**

	$t_0$ h	$t_{spall}$ h	transient mg/cm <sup>2</sup>	estimated $K_p$ mg <sup>2</sup> /cm <sup>4</sup> h	$g^2/cm^4s$	relative $k_p/k_{p,NiAl}$
Pt diffused	90	20	0.34	5.27E-02	1.46E-11	445
Pure NiAl	1290	460	0.14	1.18E-04	3.29E-14	1.0
Hf-NiAl	1770	360	0.35	9.22E-04	2.56E-13	7.8
Pt-NiAl	3620	500	0.53	6.33E-04	1.76E-13	5.3
Hf-Pt-NiAl	4070	520	0.24	7.12E-04	1.98E-13	6.0
MDC150L (on CMSX4)	N.A.	N.A.	0.10	6.50E-05	1.81E-14	0.5

400 h. This weight transient was then subtracted, leaving a remainder that could be directly compared to parabolic behavior and estimate the point of deviation.

The specific weight change behavior of all five coatings is shown in Figure 7. Figure 7a presents the entire data set and shows that all coatings exhibit typical cyclic oxidation responses. The time to cross the zero weight axis,  $t_0$ , triggered the end of the test. It can be viewed as an arbitrary, semi-quantitative indication of performance or 'life' and is presented in ascending rank in Table 2. The Pt diffused coating exhibited a rapid high weight gain and loss to zero at 90h. The simple NiAl aluminide produced a much lower weight gain and crossed zero at 1290h. The Hf-doped NiAl weights were somewhat higher and lasted until 1770h. The Pt-doped NiAl and Hf-Pt doped NiAl had similar growth rates, but extended life to 3620 and 4070h, respectively.

The parabolic growth rate,  $k_p$ , can be analyzed from the slope of isothermal  $(\Delta W/A)^2$  vs. time or  $\Delta W/A$  vs.  $t^{1/2}$  plots. Transient oxidation effects often result in an intercept at zero time on such "parabolic" plots. Pierragi has analyzed such non-idealities and showed that if the transient scales do not contribute to subsequent rate control for the stable long term oxide, then the  $t^{1/2}$  construction produces the preferable rate [56]. Conversely, if the transient scale is a transition alumina and does transform to rate controlling  $\alpha$ -Al<sub>2</sub>O<sub>3</sub>, then the preferred method employs the  $(\Delta W/A)^2$  construction [57]. Both constructions were examined in the present study and it was found that the latter produced substantial deviations from the predicted parabolic curve for the first 100 h, whereas the  $t^{1/2}$  construction produced good fits for the majority of the initial 15-400h stage of the cyclic curves (Figure 7b). These fits were also used to determine a quantity corresponding to the transient oxide by extending the lines to the abscissa at zero time, Table 2.

The parabolic rate constants corresponding to these fits are also listed in Table 2, in both practical mg<sup>2</sup>/cm<sup>4</sup>h and g<sup>2</sup>/cm<sup>4</sup>s units. It is seen that the Pt-diffused coating is over two orders of magnitude higher than that for the simple aluminide. The Pt-, Hf-, and Hf-Pt-doped aluminides are all similar and about 5-8 times that of the simple aluminide. And the commercial

Howmet MDC150L Pt-NiAl is roughly half that of the simple aluminide.

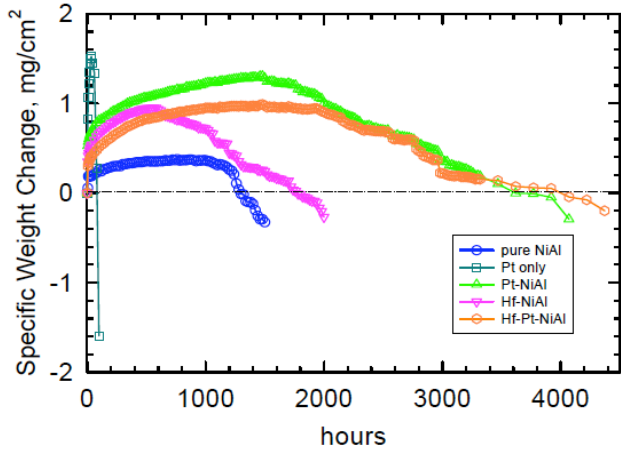
Next the raw experimental data was modified by subtracting the transient amount determined above and re-plotted along with idealized curves projected from the corresponding parabolic rates, Figure 7c. This allows for a more critical analysis of the kinetic behavior and shows that the cyclic and parabolic behavior of the aluminide coatings coincides for about the first 350-500 h. The deviation between corresponding cyclic and isothermal curves can be estimated visually and suggests where spallation may become significant. This value, referred to as  $t_{spall}$ , is presented as solid symbols on each curve and is listed in Table 2. It can be seen that while the Hf-NiAl coating deviates before the simple aluminide, it exhibits a shallower rate of final weight loss in Figure 7a. Both the Pt-NiAl and Hf-Pt-NiAl coatings have the largest  $t_{spall}$  and  $t_0$  and show similar behavior for the entire curve. The issues raised above will be significant in light of various mechanisms and the microstructural features discussed below.

### 3.3. Overall Characterization

#### 3.3.1. Optical Appearance

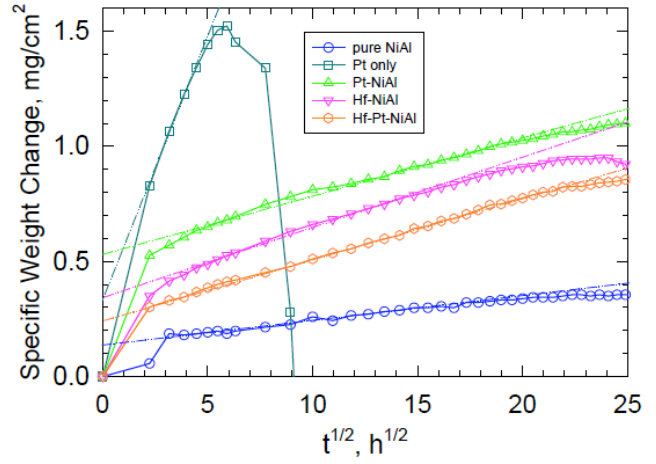
The general surface appearance is shown in the optical micrographs of Figure 8. After 100h the Pt-diffused coating was fully covered with a duplex oxide, with remnants or flakes of an outer scale layer that spalled off (Figure 8a). The simple NiAl coating after 1500 h, Figure 8b, exhibited jigsaw morphology of bright reflective areas, a light grey oxide, and a medium tan-ochre oxide. The characteristic dimension was on the order of 25  $\mu$ m, or similar to the 20-40  $\mu$ m prior grain size of the coating. The same was true for the Pt-NiAl coating after 4070h, Figure 8d, but with more area of exposed metal, more area of uniform light grey scale, and a distinctive network pattern. Here the characteristic dimension was 20  $\mu$ m, compared to that of the original 5-10  $\mu$ m of the surface cusps. However, the Hf-NiAl coating shown after 2000 h in Figure 8c, possessed features that were ~ 100-200  $\mu$ m, more uniformly distributed, and not reflective of the prior 10-20  $\mu$ m coating grain boundary network. Lastly, the same description

**1050°C Oxidation of Sifco NiAl (Pt,Hf) on IN-718**  
Cyclic Furnace Test, 20 hr/cycle



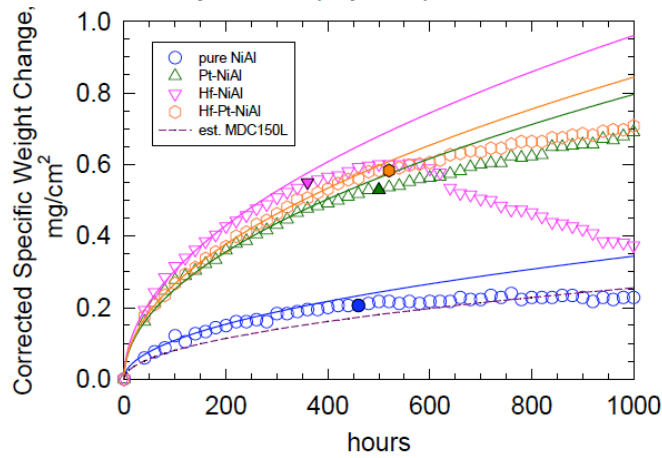
(a)

**1050°C Oxidation of Sifco NiAl (Pt,Hf) on IN-718**  
Cyclic Furnace Test, 20 hr/cycle



(b)

**1050°C Oxidation of Sifco NiAl (Pt,Hf) on IN-718**  
Cyclic Furnace Test, 20 hr/cycle  
adjusted and projected parabolic



(c)

**Figure 7:** 1050°C cyclic oxidation weight change behavior of coatings on Inconel 718.

a) Specific weight change vs time; b) Specific weight change vs  $t^{1/2}$  parabolic plots; c) Transient-corrected cyclic curves (open symbols) compared to parabolic projections (no symbols); solid points indicate deviation of cyclic and isothermal curves.

applies to the Hf-Pt-NiAl coating shown after 4370h in Figure 8e.

### 3.3.2. X-Ray Diffraction Results

The surfaces of the oxidized samples were analyzed by X-ray diffractometer scans after the tests were completed. The resulting metal and scale phases are listed in Table 3. The numerical values are semi-quantitative estimates of the relative wt. % of the surface phases, using a commercial software program and assuming a uniform distribution and random crystallographic orientations. All the samples revealed a considerable amount of metal phase, as exposed by spalling or detected under the scale thickness. These were characterized as  $\gamma$ -Ni<sub>soln.</sub> and/or  $\gamma$ -Ni<sub>3</sub>Al, with some ambiguity because of the weakness of the discerning

superlattice peak and its overlap with peaks from the rhombohedral corundum structures. The quantity of metal phase decreased with coatings ordered by increasing time to reach zero weight gain. This is consistent with thicker scales and absorption as well as less area of bare metal exposed by spalling.

The Pt diffused coating produced primarily  $\alpha$ -Cr<sub>2</sub>O<sub>3</sub> and TiNbO<sub>4</sub> rutile scales, in nearly equal amounts. The other coatings produced primarily  $\alpha$ -Al<sub>2</sub>O<sub>3</sub> scales, with minor amounts of Ni(Al,Cr)<sub>2</sub>O<sub>4</sub> spinel and variations of TiO<sub>2</sub> or CrNbO<sub>4</sub> rutile structures. The observed d-spacings of the spinel solid solution phases are listed, considering that those of NiAl<sub>2</sub>O<sub>4</sub> and NiCr<sub>2</sub>O<sub>4</sub> are 8.05Å and 8.35Å, respectively. Similarly, the a and c lattice parameters of the rutile phases

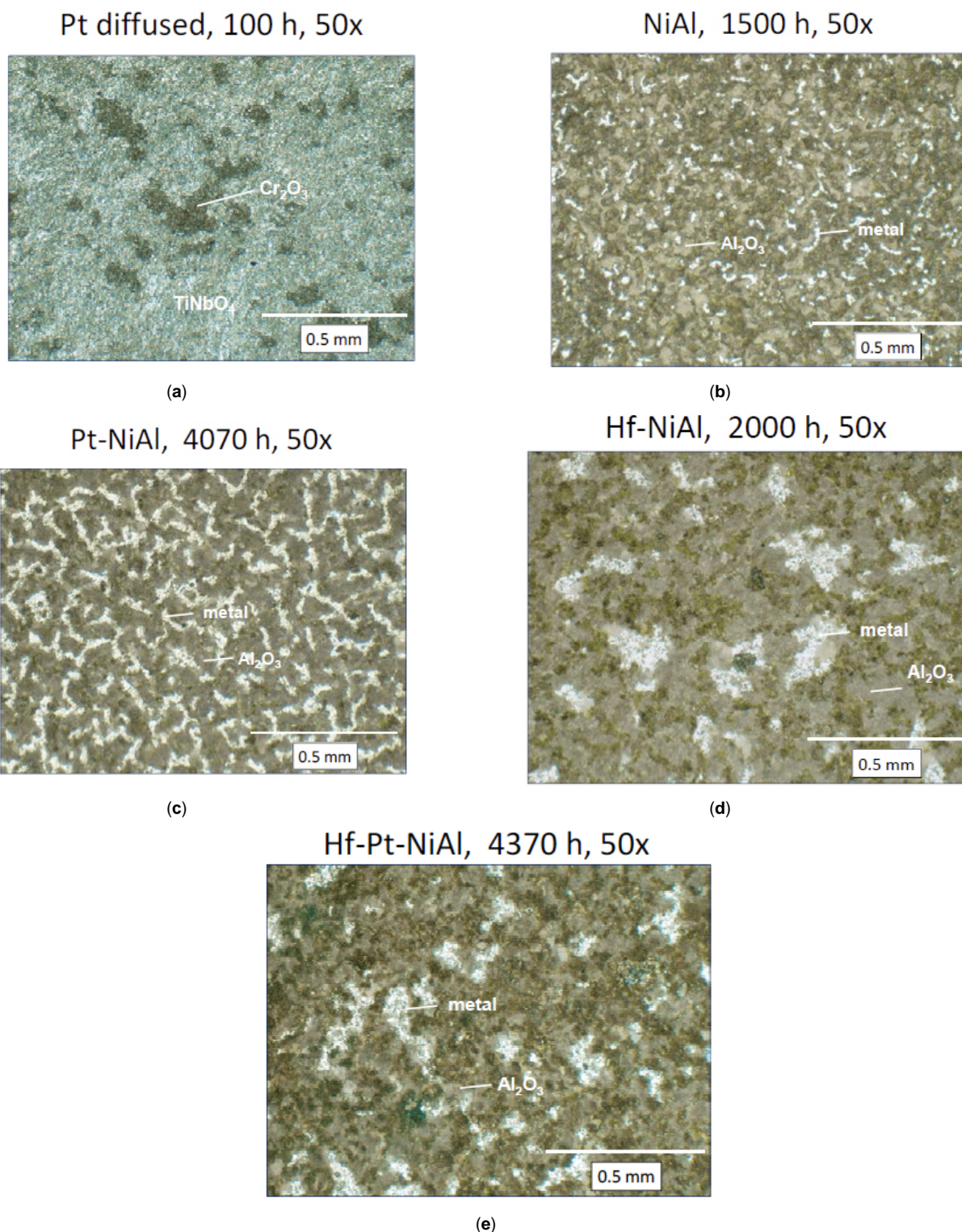


**Figure 8:** General coating surface and scale appearance at the end of 1050°C cyclic oxidation tests. (low magnification optical micrographs;). a) Pt-diffused coating, 100 h; b) Simple NiAl, 1500 h; c) Hf-NiAl, 2000 h; d) Pt-NiAl, 4070 h, e) Hf-Pt-NiAl, 4370 h.

may vary over Ti, Nb, Cr, Ni solid solutions, where those of TiNbO<sub>4</sub> are 4.72 Å and 3.00 Å, respectively.

### 3.3.3. Coating Composition

This topic will be addressed below, but it is helpful to first point out some overall trends. The EDS characterization of

the coating composition is summarized before and after testing in Table 1. It is seen that all the aluminide coatings exhibit a dramatic drop in Al content, decreasing from ~30 wt.% initially down to as low as 2 wt.%, while increasing in Nb content from zero to ~5 wt.%. The three Pt and Hf doped aluminides also exhibited ~15 wt. % Cr and Fe at the end of

**Table 3: Surface Phase Content of Coatings on Inconel 718 after Cyclic Oxidation at 1050°C. (wt. %, Semi-Quantitative). Spinels and Rutilites may have Various Compositions that Produce the Same Lattice Parameters**

1050°C coating	time hours	weight mg/cm <sup>2</sup>	metal	alumina	chromia	spinel		rutilites				
			γ/γ'	α-Al <sub>2</sub> O <sub>3</sub>	α-Cr <sub>2</sub> O <sub>3</sub>	Ni(Al,Cr) <sub>2</sub> O <sub>4</sub>	Å	Ti(Nb)O <sub>4</sub>	TiNbO <sub>4</sub>	CrNbO <sub>4</sub>	HfO <sub>2</sub>	
Pt diffused	100	-1.59	32		35			3	30			
NiAl	1500	-0.33	51	45		2	8.17	2				
Hf-NiAl	2000	-0.27	38	54		2	8.15				2	3
Pt-NiAl	4070	-0.29	32	66		2	8.15				1	
Hf-Pt-NiAl	4370	-0.20	24	63		9	8.12	3				2

testing. These changes may be responsible for significant effects on oxidation.

**3.4. Detailed SEM/EDS Characterization**

SEM/EDS studies of the oxidized surface were made at 100, 500, 1500, 2000, 2560, 4070, and 4370 h, depending on the particular coating and whether it survived that long. The series presented below used primarily backscatter imaging (BSE) for discrimination by atomic weight.

**3.4.1. Pt-Diffused Coating**

Exposure of the Pt coated specimen was stopped after 100h testing. The weight change had already gone through its maximum, crossed zero, and achieved a loss of ~1.5 mg/cm<sup>2</sup>. The microstructure of the oxidized specimen surface in Figures 9a and 9b shows an intertwined mixture of dark and light phases, but perhaps at a different area ratio than the features in Figure 8a. Three different areas are indicated by contrast and EDS: the dark area (“A” in Figure 9b) was chromium oxide, expected to be α-Cr<sub>2</sub>O<sub>3</sub>; the gray area (“B”

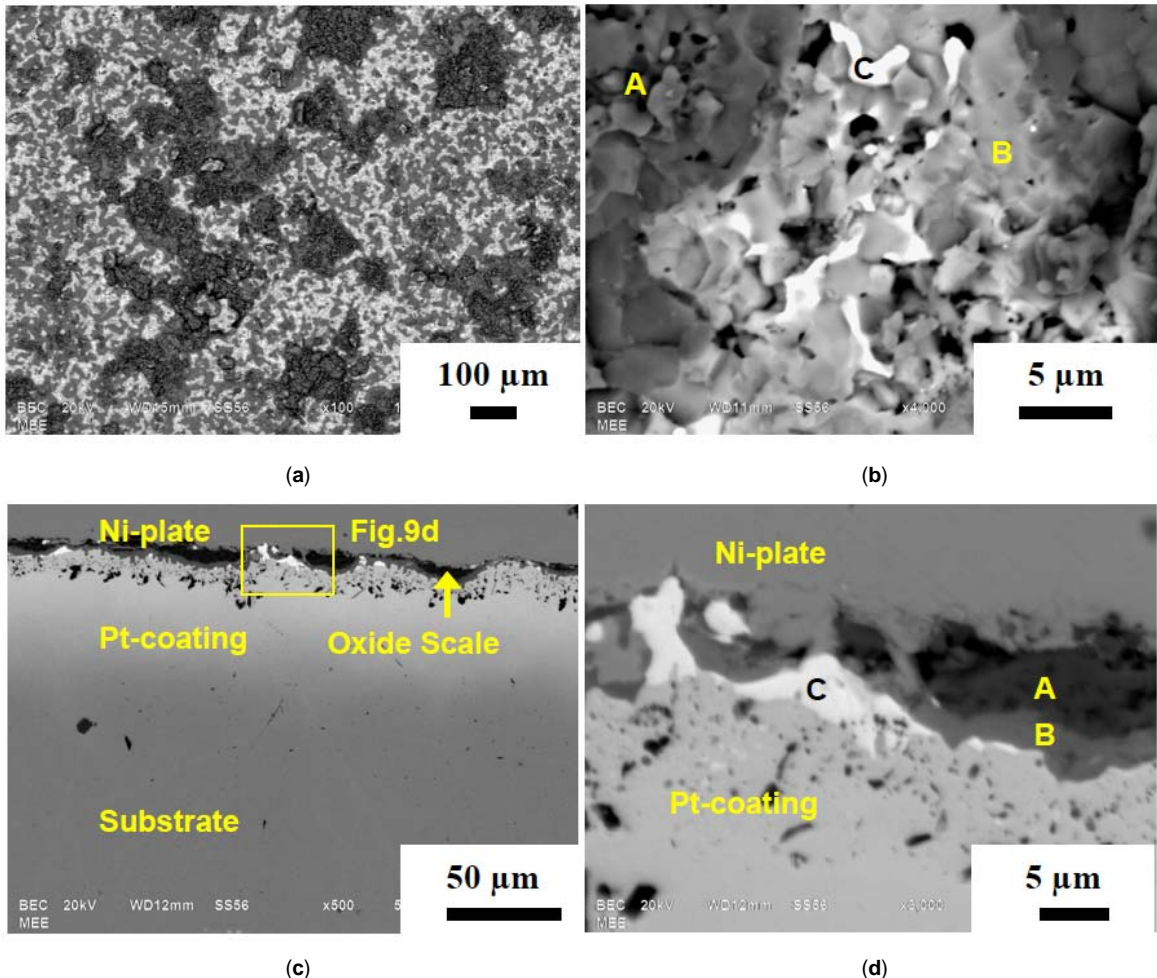
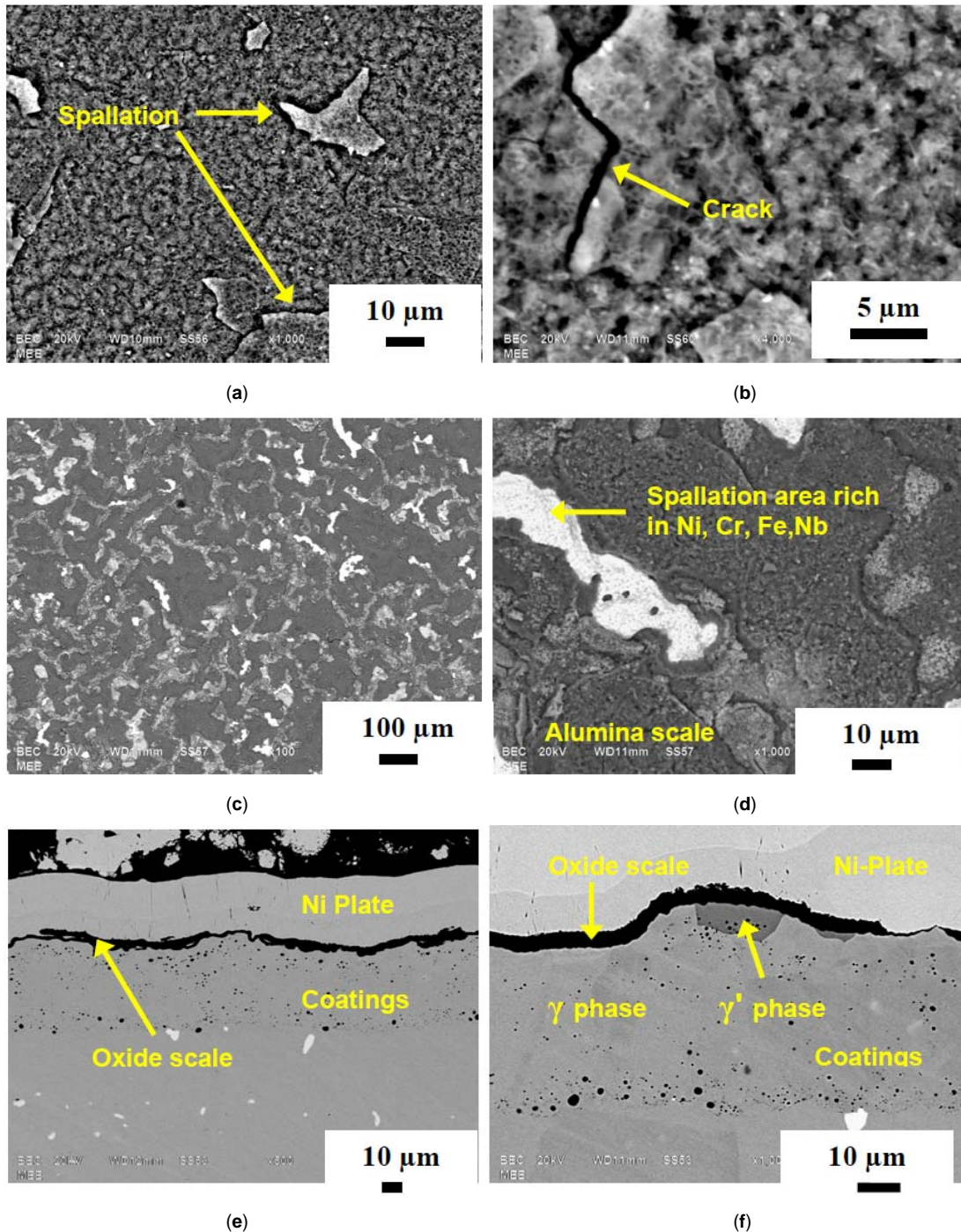


**Figure 9: SEM backscattered electron micrographs of the Pt-diffused coating after 100h oxidation at 1050°C. (a) and (b) Surface morphology, (c) and (d) Cross-section.**

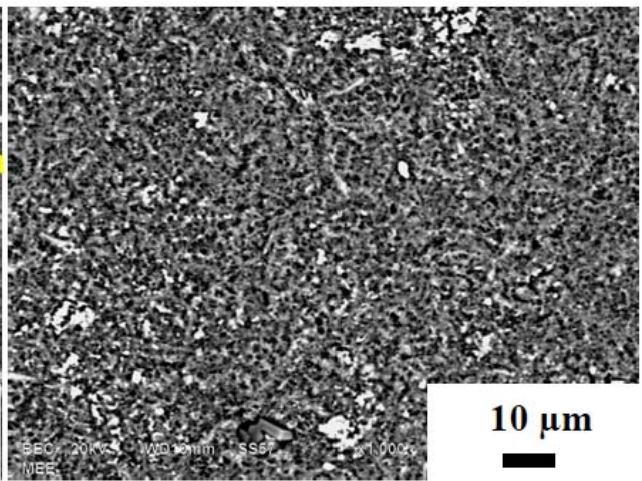
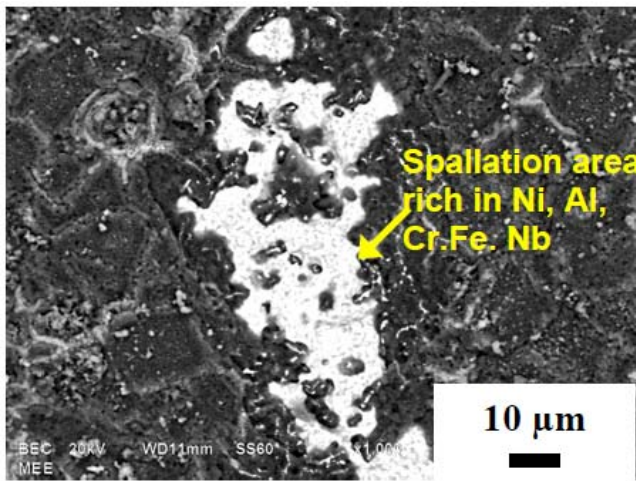
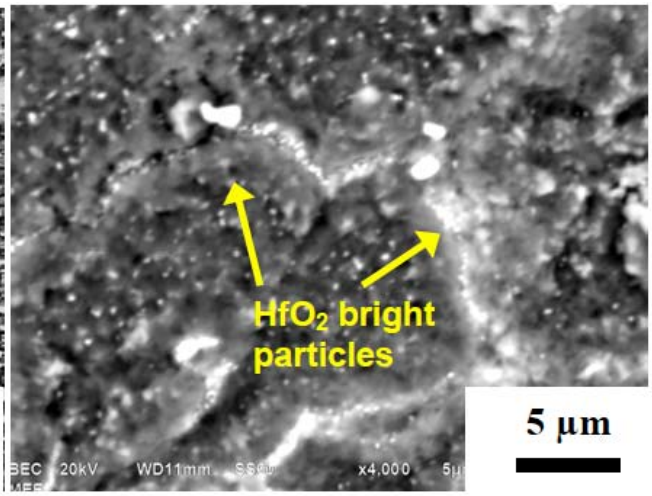
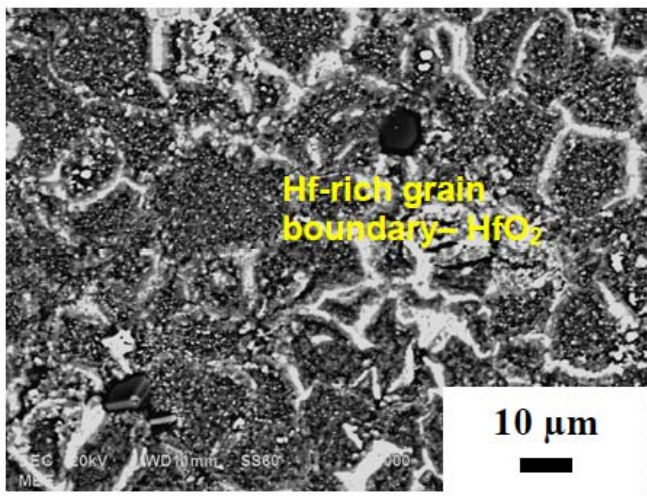
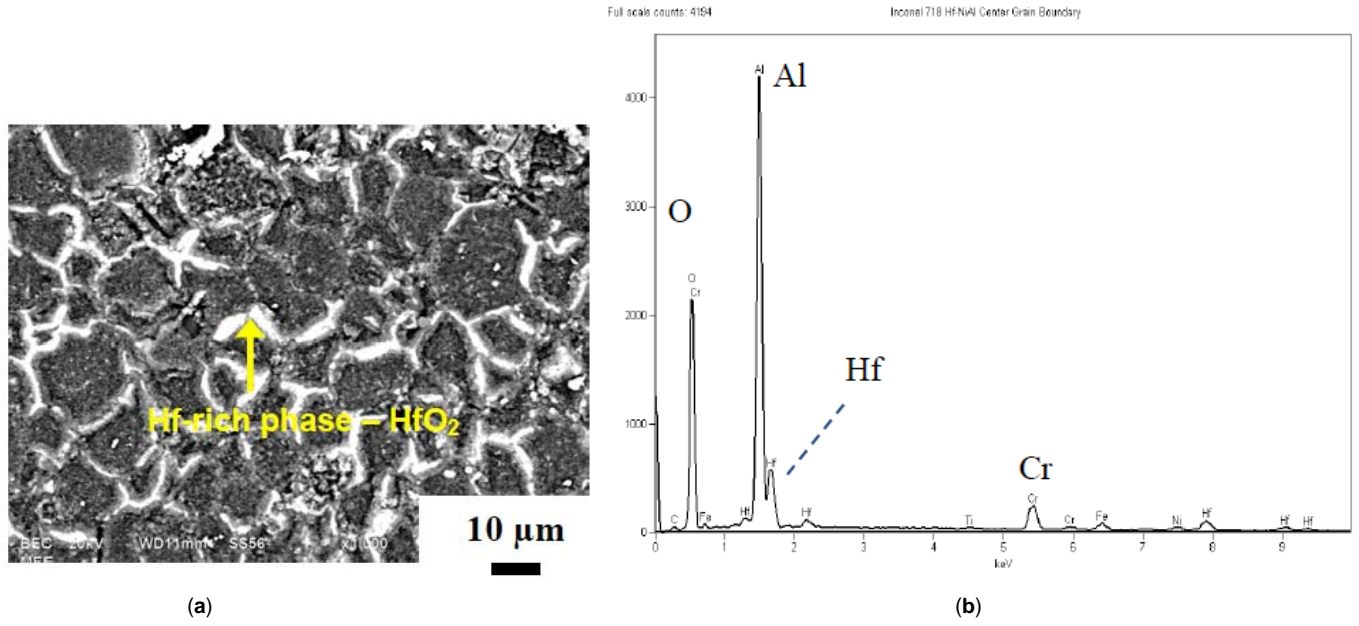
in Figure 9b) was niobium-rich oxide (a form of the (Ti,Cr)NbO<sub>4</sub> rutiles); and the brightest phase ("C" in Figure 9b) was Pt-rich metal. Similarly, the scale exhibited three regions in cross-section (Figures 9c and 9d): the outer dark area, "A", the gray area, "B", and the bright phase, C, were chromium oxide, niobium-rich oxide, and Pt-rich phases, respectively, consistent with the surface structure. The chromium oxide layer thus appears to be an outer layer that has spalled in many areas. It was also found that the initial Pt layer diffused an additional ~25 μm into the alloy.

### 3.4.2. NiAl Coating

The NiAl-coated specimen was inspected by SEM/EDS at 100h, 500h, and 1500h, at which point the test was stopped, Figure 10. After 100h oxidation, an Al-rich oxide, presumably α-Al<sub>2</sub>O<sub>3</sub>, was present with cracks and spalled flakes (Figure 10a). Local scale spallation, found in one corner, was analyzed to be rich in Ni, Cr, Nb, etc., with no oxygen, indicating exposed metal. After 500h, the Al<sub>2</sub>O<sub>3</sub> scale remained mostly adherent, but spalled flakes and cracks in



**Figure 10:** SEM of the simple NiAl coating oxidized at 1050°C. Surface morphology (a) after 100h, (b) after 500h, (c) and (d) after 1500h testing, and cross-section (e) and (f) after 1500h.



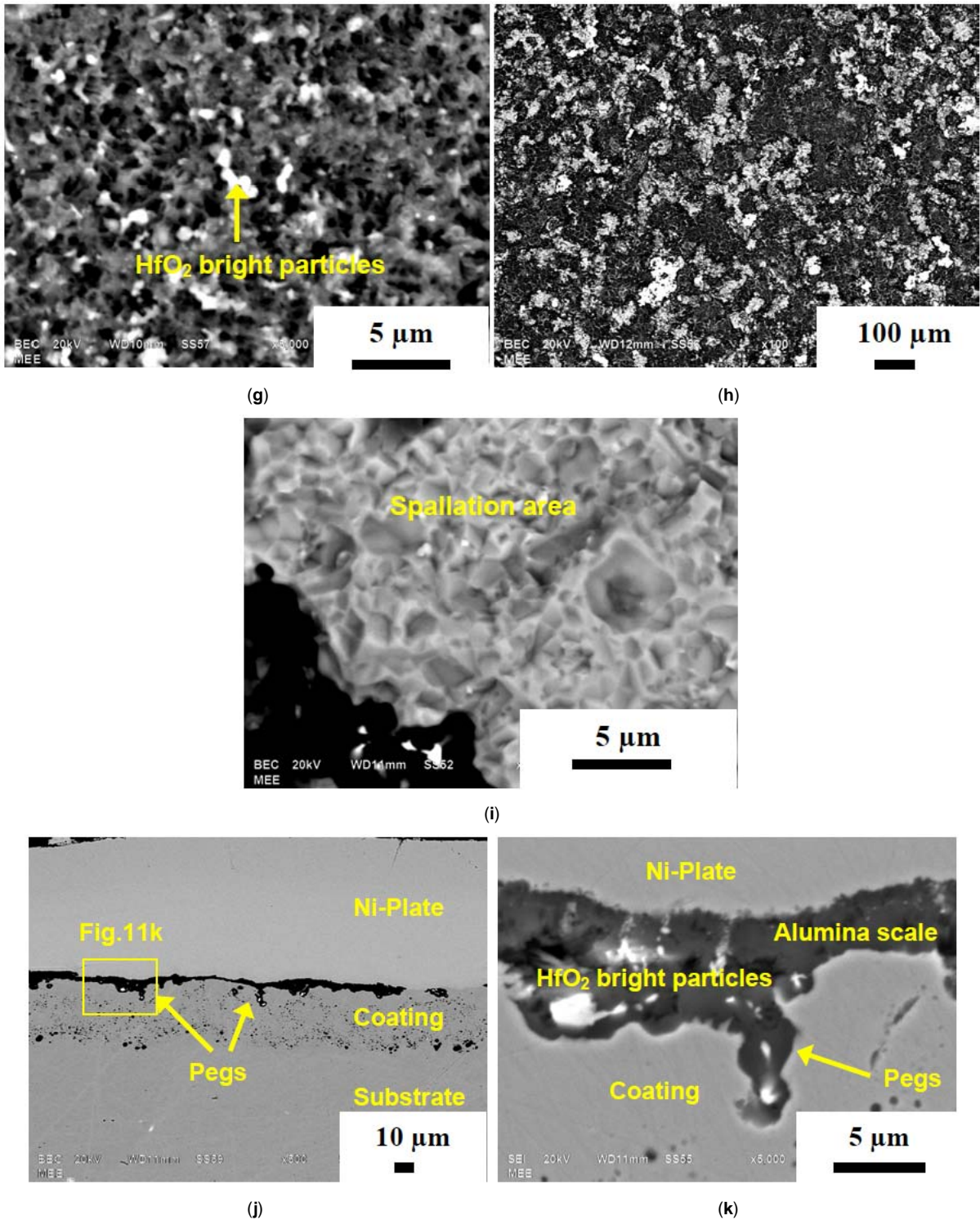


**Figure 11:** SEM backscattered electron micrographs of the Hf-NiAl coating oxidized at 1050°C. Surface (a) after 100h; (b) EDS spectrum obtained from a grain boundary; (c) (d), and (e) after 500h; (f) and (g) after 1500h; (h) and (i) after 2000h; and cross-section (j) and (k) after 2000h.

the retained scale were again found (Figure 10b). This is consistent with deviation from the predicted isothermal behavior occurring at ~460 h. Finally, after 1500h exposure, an extensive 'river' network of bright, exposed metal spalled areas and grey oxide was apparent (Figures 10c and 10d).

The bright metal areas were again rich in Ni, Cr, and Nb, with no oxygen. The grey phases were rich in Ni, Al, Cr, and O, presumably Ni(Al,Cr)<sub>2</sub>O<sub>4</sub> spinel. The dark circumscribed islands were remnant Al-oxide. The bare metal appeared more as a uniform dispersed phase in the final optical

micrograph, Figure 8b. But here it is seen associated with the spinel scale in an associated network pattern. It can be surmised that the spinel network represents re-oxidized bare metal from prior cycles, and that both together portray a pattern where spalling was preferred, perhaps associated with the rumpling patterns. The weight change at this time was a loss of 0.3 mg/cm<sup>2</sup>.

Surface undulations or rumpling were clearly seen in the NiAl cross-section (Figures 10e, f). In addition, islands of a gray phase (Figure 10f) were formed in the coating just below the Al<sub>2</sub>O<sub>3</sub> scale. The island was analyzed by EDS to be 67.5Ni-16.8Al-5.1Cr-8.0Fe-1.0Ti-1.6Nb (wt. %), indicating the  $\gamma'$ -Ni<sub>3</sub>Al phase, while the surrounding matrix was 72.9Ni-8.2Al-3.2Cr-6.6Fe-2.2Ti-6.9Nb, indicating  $\gamma$ -Ni solid solution. Both are consistent with XRD results. The transformation from the original  $\beta$ -NiAl into  $\gamma'$ -Ni<sub>3</sub>Al and  $\gamma$ -Ni was caused by Al depletion due to the formation and spallation of Al<sub>2</sub>O<sub>3</sub> scales and interdiffusion with the substrate.

### 3.4.3. Hf-NiAl Coating

The Hf-NiAl coated specimen was examined by SEM/EDS at 100h, 500h, 1500h, and 2000h exposures, at which point testing was halted. At 100h, the dense base scale was primarily Al<sub>2</sub>O<sub>3</sub>, while the Hf-rich coating grain boundaries were highly delineated (Figure 11a, b). The bright ridges and the small Hf-rich bright particles are expected to be HfO<sub>2</sub> [39], as shown by XRD. This would be consistent with results for Hf-doped bulk NiAl, where HfO<sub>2</sub> particles are observed to grow at the outer surface of Al<sub>2</sub>O<sub>3</sub> [29]. After 500h, the Al<sub>2</sub>O<sub>3</sub> scales remained adherent for the most part (Figure 11c), again with HfO<sub>2</sub> bright particles decorating the coating grain boundaries (Figure 11d). However, some localized spallation was found in the corner area of the specimen (Figure 11e). This is consistent with deviation from the predicted isothermal curve occurring earlier at ~360 h. The spalled region was rich in Ni, Al, Cr, Fe, Nb, but no oxygen, indicating metal exposed by interfacial alumina scale spallation.

After 1500h, the weight change was well past the maximum of 0.9 mg/cm<sup>2</sup> at ~600 h, falling to 0.2 mg/cm<sup>2</sup> and tending toward zero weight change. Spallation continued at corner areas, but the scale was still adherent in most areas, Figure 11f. Finely dispersed, bright HfO<sub>2</sub> particles, Figure 11g, were also present, yet the pattern of coating grain boundary decoration was supplanted by a more uniform distribution of features. Coupled with weight loss, this suggests that interfacial spallation occurred at least once over the entire sample, leaving an altered, re-healed structure with no evidence of the original scale. After 2000h exposure, the surface structure showed a dispersed mixture of intact  $\alpha$ -Al<sub>2</sub>O<sub>3</sub>, spallation, and bright HfO<sub>2</sub> particles, Figure 11h, consistent with XRD results. The HfO<sub>2</sub> particles were estimated to be less than 100 nanometers in diameter. The spallation area exhibited the characteristic imprints of the spalled  $\alpha$ -Al<sub>2</sub>O<sub>3</sub> grains (Figure 11i) and was rich in Ni, Cr, Fe, Al, Nb and Mo, with no oxygen. The overall spalling

distribution was resolved more clearly in the optical micrograph of Figure 8e, showing there a uniform distribution of 100-200  $\mu$ m patches of spalled regions. At this point the coating had reached -0.3 mg/cm<sup>2</sup>.

The polished cross-section (Figure 11j) showed less surface rumpling compared with the failed NiAl coat. The coating composition, Table 1, was 55.1Ni-2.6Al-16.5Cr-17.1Fe -1.1Ti-5.0Nb-2.6Mo (wt. %), indicating that the initial  $\beta$ -NiAl phase had completely transformed into  $\gamma$ -Ni<sub>soln</sub>, as indicated by XRD. Cr, Fe, and Nb content increased considerably. Oxide pegs were observed, and their morphology at high magnification, Figure 11k, indicates bright HfO<sub>2</sub> particles surrounded by Al<sub>2</sub>O<sub>3</sub>. The size of the HfO<sub>2</sub> particles varied from less than 100 nanometers to several micrometers (~2.5  $\mu$ m max.).

### 3.4.4. Pt-NiAl Coating

The exposure of the Pt-NiAl coat specimen was inspected at 100h, 500h, 1500h, 2560h, and after stopping at 4070h exposures. At 100h, the dense Al<sub>2</sub>O<sub>3</sub> oxide scale reflected the cusped, ridge structure of the coating and exhibited no spallation (Figure 12a). The fine bright particles along these ridges were rich in Nb, presumably as Nb-containing rutile embedded in alumina. After 500h, the same ridge features were seen except that the size of the bright Nb-rich particles increased, (Figure 12b). At 1500h, a large number of cracks were formed in the alumina scale (Figure 12c), but with no apparent spallation. Even though the weight change had begun to deviate from projected isothermal response at 500 h, it was still gaining weight up to 1470 h. At 2560h, significant spallation had occurred (Figure 12d), leading to a loss of about 1/2 the maximum gained. The spalled regions again showed the typical polygonal alumina grain imprint structure in exposed metal, rich in Ni, Al, Nb, Pt, Cr, and Fe, with no oxygen. After 4070h, the scale surface showed more spallation (Figure 12e), and alumina scales decorated with bright Nb-rich oxide particles (Figure 12f). Other light grey areas starting at 1500 h and seen increasingly here appeared to be previously spalled and re-healed areas, showing an Al, Ni, Cr-rich scale, presumably Ni(Al,Cr)<sub>2</sub>O<sub>4</sub> spinel. These results reflect the XRD identification of  $\alpha$ -Al<sub>2</sub>O<sub>3</sub>, spinel, and CrNbO<sub>4</sub> rutile. However, it estimated a lower quantity of spinel and more Cr in the rutile than expected.

In the low magnification optical micrograph, Figure 8d, it was seen that the spalled regions formed a distinctive but disconnected pattern with perhaps some relationship to the highly cusped network of the original coating structure. But, interestingly, the spalled features here exhibit a characteristic dimension and spacing that is ~200  $\mu$ m or many times greater than that of the ~5  $\mu$ m coating cusp features. They may thus correspond to a rumpling dimension, with outlines somewhat defined by the fine cusp features.

In cross-section, the oxidized surface showed significant rumpling (Figure 12g, with the fine Nb-rich oxide bright particles embedded in the alumina layer (Figure 12h). The Pt-

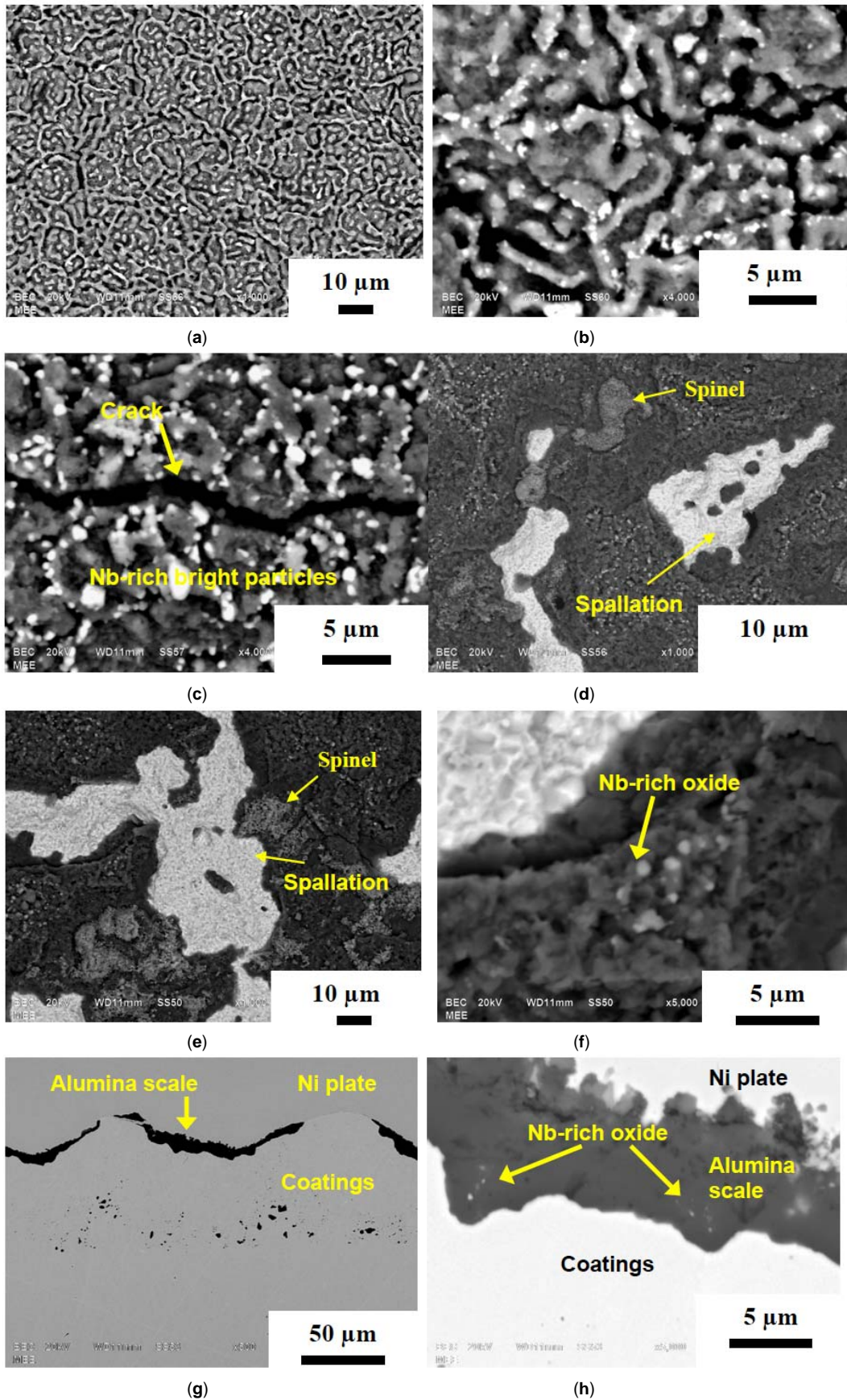


**Figure 12:** SEM backscattered electron of the Pt-NiAl coating oxidized at 1050°C. Surface (a) after 100h; (b) after 500h; (c) after 1500h; (d) after 2560h; (e) and (f) after 4070h, and cross-section (g) and (h) after 4070h.

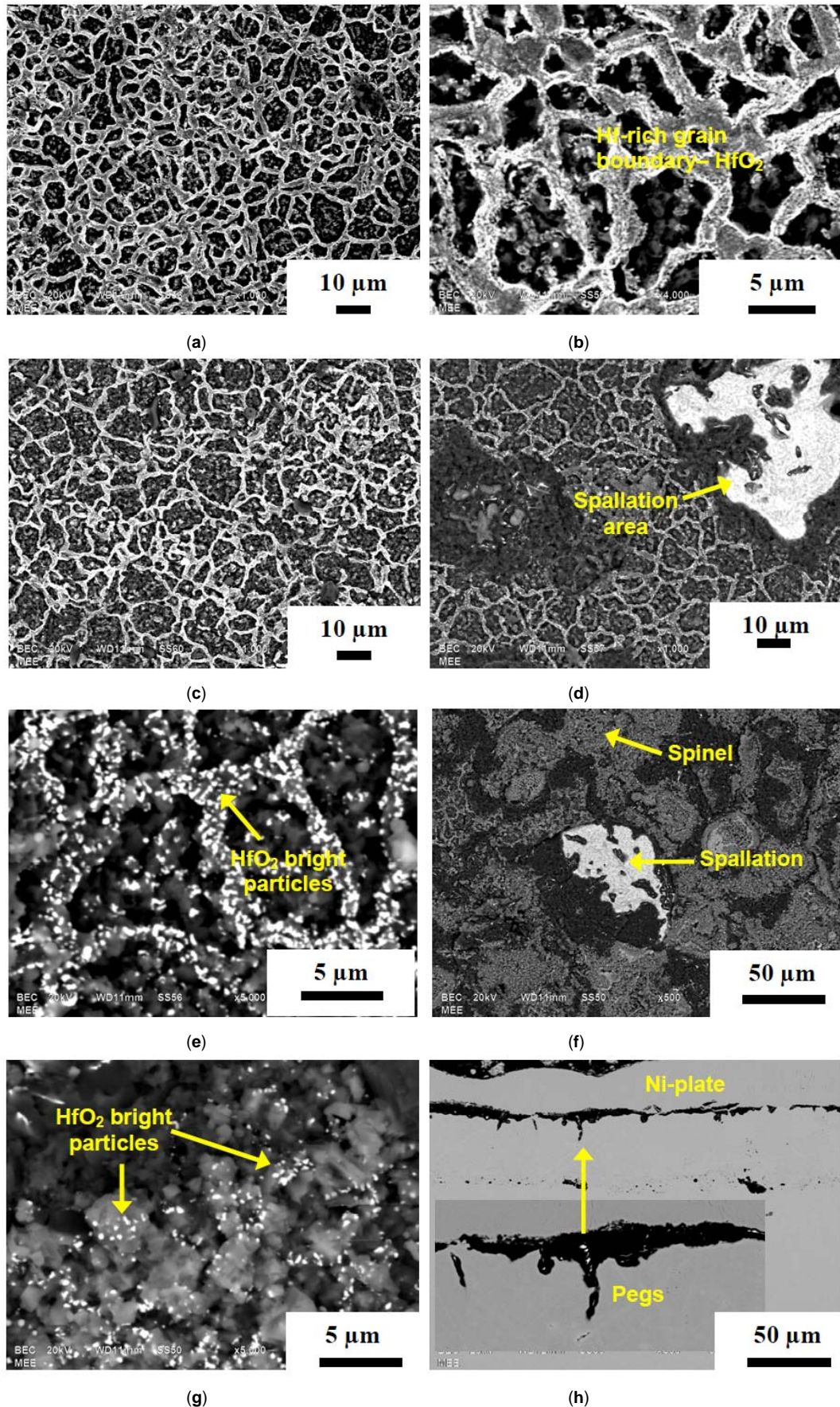


**Figure 13:** SEM backscattered electron micrographs of the Hf-Pt-NiAl coating oxidized at 1050°C. Surface (a and b) after 100h; (c) after 500h; (d) after 1500h; (e) after 2560h; (f and g) after 4370h; and cross-section (h) after 4370h.

NiAl coatings showed a composition about 2 $\mu$ m below the alumina scale of 54.1Ni-3.6Al-15.2Cr-15.1Fe -1.1Ti-4.9Nb-6Pt (wt. %). This confirms XRD showing substantial transformation from the original  $\beta$ -(Ni,Pt)Al +  $\xi$ -PtAl<sub>2</sub> to  $\gamma$ -Ni<sub>soln</sub>, and indicates the incorporation of Cr, Fe, Nb, and Ti.

**3.4.5. Hf-Pt-NiAl Coating**

The Hf-Pt-NiAl coating was inspected by SEM at 100h, 500h, 1500h, 2560h, and after terminating at 4370h. At 100h, dense Al<sub>2</sub>O<sub>3</sub> oxide scales were formed with no apparent spallation (Figure 13a). The distinct Hf-rich ridge structure of the coating was emphatically replicated by bright particles as a Hf-rich oxide, presumably HfO<sub>2</sub> (Figure 13b) [39]. The same features were maintained after 500h (Figure 13c). Spalling and deviation from the projected isothermal weight curve was projected to start at 520 h, so adherent scales were expected. However, after 1500h the weight change has just reached its maximum. Localized spallation is now observed with individual spall segments spanning a number of the prior ridge features (Figure 13d). The same general structure was observed after 2560h, but now with a more distinctly coarsened HfO<sub>2</sub> particulate, (Figure 13e). The bright spalled areas were rich in Ni, Al, Nb, Pt, Cr, and Fe, (but no oxygen) indicating the exposed metal surface of the coating. The weight change was in a steady linear decline at this point. Finally, after 4370h, spallation continued such that large areas of spalled and re-oxidized surfaces were evident as grey Ni, Cr-rich scales in contrast to dark Al<sub>2</sub>O<sub>3</sub>, Figure 13f. This is somewhat consistent with XRD results showing  $\alpha$ -Al<sub>2</sub>O<sub>3</sub>, spinel, and Ti(Nb)O<sub>2</sub> rutile. The fine, bright HfO<sub>2</sub> particles were still present, as confirmed by XRD, but now positioned on top of a base of grey spinel scale (Figure 13g). At lower magnification, the optical micrograph of the oxidized surface showed less degree of spalling than the Pt-NiAl coating, Figures 8d and e, and in a more random pattern.

The polished cross-section showed that the surface was relatively flat (Figure 13h), with less rumpling compared to the failed Pt-NiAl coatings. As with the Hf-NiAl coating without Pt, Al<sub>2</sub>O<sub>3</sub> oxide pegs were observed with bright HfO<sub>2</sub> particles

inside. The coating composition was 53.6Ni-2.2Al-16.6Cr-16.8Fe-1.1Ti-4.4Nb-5.3Pt (wt. %) about 2 $\mu$ m below the alumina scale interface. The original Hf-Pt-modified  $\beta$ -(Ni,Pt)Al coating transformed into  $\gamma$ -Ni<sub>soln</sub>, as confirmed by XRD, with considerable increase in Cr, Fe and Nb content.

**4. DISCUSSION**

The Pt diffused coating failed in less than 100h because of the low Al content in this system and the formation of Cr<sub>2</sub>O<sub>3</sub> instead of Al<sub>2</sub>O<sub>3</sub> scales. Cr<sub>2</sub>O<sub>3</sub> scales grow faster and are more susceptible to spallation at temperatures ~1000°C and degrade by volatilization of Cr<sub>2</sub>O<sub>3</sub> (s) to CrO<sub>3</sub> (g) [58-59]. Though ineffective on Inconel 718, diffused Pt coatings are quite successful on higher aluminum Ni-base superalloys where Al<sub>2</sub>O<sub>3</sub> scales can be formed on  $\gamma$ -Ni +  $\gamma'$ -Ni<sub>3</sub>Al two-phase alloys [32].

In contrast with the Pt-coating, the other four coatings showed significantly better oxidation resistance. The coating lifetime, arbitrarily defined as the oxidation testing time to zero weight change, was summarized in Figure 14a. The addition of Hf to the NiAl and Pt-NiAl coatings increased the lifetime ~37% (from 1296h to 1775h) and 11% (from 3614h to 4001h), respectively. Alternatively, the coating lifetime depends on the oxidation behavior of the surface composition as well as the coating thickness and Al reservoir. If the coating thickness is considered, Hf additions increased the normalized coating lifetime ~46% (from 20.9 h/ $\mu$ m to 30.6 h/ $\mu$ m) and ~58% (from 35.8 h/ $\mu$ m to 56.4 h/ $\mu$ m), respectively, Figure 14b. This approximate ranking suggests that Hf-Pt-NiAl > Pt-NiAl > Hf-NiAl > NiAl > Pt-diffusion coatings. The beneficial effect of Hf-doping is in an agreement with the previous studies on Hf-doped cast NiAl alloys [25, 29, 31], though our present results represent only a limited number of samples.

The parabolic oxidation rate constant  $k_p$  can be represented by [56]:

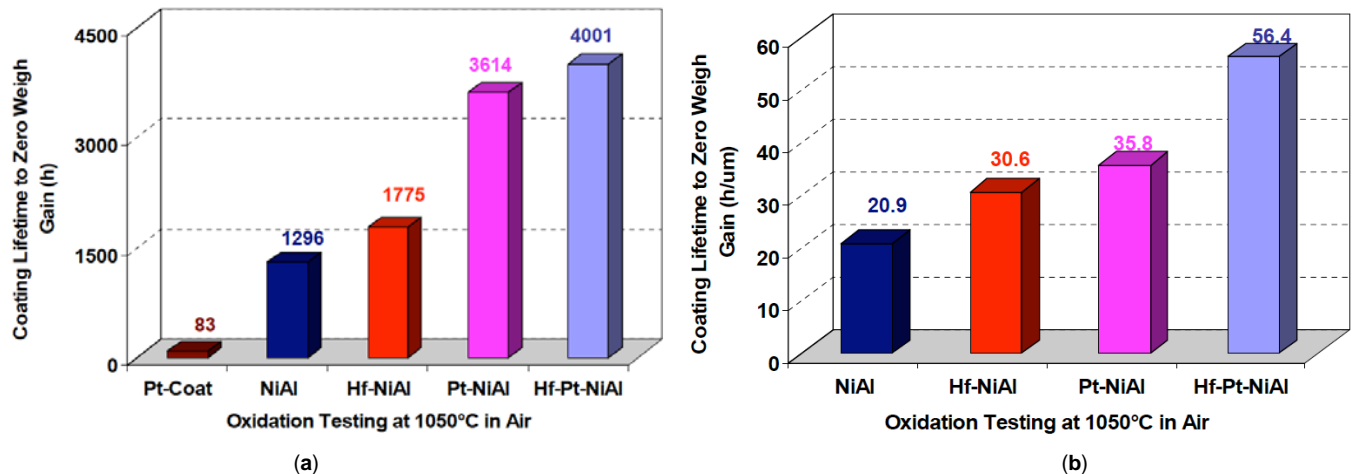


Figure 14: Coating lifetime to zero weight gain at 1050°C (a) Raw lifetime; (b) Lifetime normalized by coating thickness.

$$(\Delta m - \Delta m_i)^2 = k_p(t - t_i) \quad (1a)$$

$$\Delta m - \Delta m_i = \left\{ k_p(t - t_i) \right\}^{1/2} \quad (1b)$$

where  $\Delta m$  is the weight change at time  $t$ , and  $\Delta m_i$  is the weight change associated with the transient period  $t_i$  of initial fast oxidation into steady state oxidation. In equation (1), the initial weight gain is corrected out to allow calculation of the parabolic rate constant. Better parabolic fits were obtained by eqn. 1b, as discussed in section 3.1 and summarized in Table 2. The results indicate similar  $k_p$  for the Pt, Hf, and Hf-Pt-doped aluminide coatings. Interestingly enough, however, these values were all greater than that for the simple aluminide, which, in turn, was above that for the commercial MDC150L Pt-modified aluminide. An optimally doped Hf-NiAl coating should decrease  $k_p$  significantly. The high rates obtained here can be attributed to excess  $\text{HfO}_2$  formation from the 0.3-0.4 wt. % Hf coating surface and additional internal oxidation as  $\text{HfO}_2$ -initiated oxide pegs. It is more difficult to explain the high rate of the Pt-NiAl coating. Perhaps it was associated with the increased cusped surface area or some undesirable effect of the  $\text{PtAl}_2$  second phase.

The composition of the Hf-NiAl coating prior to testing was around Ni-32.0Al-7.5Cr-15.3Fe, with  $\sim 0.1$  Hf<sub>avg.</sub> (wt. %). It has been reported [29] that the 1100°C parabolic rate constants  $k_p$  from cast bulk alloys of NiAl-5Cr-0.05 at. %Hf (Ni-29.5Al-6.0Cr-0.2Hf, wt.%) and NiAl-0.05 at.%Hf (Ni-31.5Al-0.2wt.% Hf) were  $4.3 \times 10^{-13}$  g<sup>2</sup>/cm<sup>4</sup>/sec and  $\sim 0.8 \times 10^{-13}$  g<sup>2</sup>/cm<sup>4</sup>/sec, respectively. These are compatible with the present value of  $2.6 \times 10^{-13}$  g<sup>2</sup>/cm<sup>4</sup>/sec, considering the 50°C temperature differential and secondary element (Fe, Ti, Nb) compositional differences that developed (Table 1).

Regarding scale adhesion, it would be expected that Hf-doping should dramatically improve cyclic behavior compared to the simple aluminide. Accordingly, minor spallation was observed on the NiAl coating after just 100h, but not on the Hf-NiAl coating until the 500h examination. Yet deviations from projected parabolic curves and the maximum in weight gain occurred at an earlier time for the Hf-NiAl coating, with a somewhat lower rate of weight loss.

Similar comparisons can be drawn for the Pt-NiAl and Hf-Pt-NiAl coatings. Both deviate from their projected parabolic rate ( $\sim 500$  h) and reached a maximum (1500 h) at similar times. At 1500 h the Pt-NiAl coating only showed cracks in the alumina scales, while the Hf-Pt-NiAl coating already showed spallation. But then the Pt-NiAl coating lost weight more rapidly, eventually following similar curves.

To some extent then the Hf-doped coatings did not exhibit unequivocal, dramatic improvements in scale growth and adhesion as might be expected from the bulk studies. The high concentration of Hf in the coating surface resulted in a high concentration of  $\text{HfO}_2$  particles at coating grain boundaries and within the scales, sized from less than 100

nanometers to several microns. Furthermore, Hf played a role in the initiation and growth of  $\text{Al}_2\text{O}_3$  intrusions into the metal. This all contributed to an excess in weight gain, though the average thickness may not have been affected as much. To some extent, the production of oxide intrusions may increase stress concentrations in the scale on cooldown and increase spallation. The various phenomena have been described in terms of "over-doping" [60]. Furthermore, the  $\sim 30$  ppmw S substrate impurity may have been too much for Hf-doping to completely overcome.

Pegging has long been associated with reactive element effects and associated with scale adhesion, though not necessarily proven as cause and effect. Similar Hf-induced oxide pegs have been reported on Hf-doped Co-10 Cr-11Al (wt. %) cast alloys [20, 22], Hf-doped NiAl cast alloys [25], and 70Ni20Al7Cr3Hf (wt. %) cladding alloys on a Rene 80 substrate [61]. Pegging is thought to be a special borderline case of internal oxidation where oxygen in solution can form  $\text{HfO}_2$  first, due to its high oxygen affinity ( $-\Delta G^\circ$  of oxide formation) [62], even underneath a newly formed  $\text{Al}_2\text{O}_3$  layer. But rapid oxygen diffusion in  $\text{HfO}_2$  relative to  $\text{Al}_2\text{O}_3$  allows further penetration, primarily at regions connected to the surface. Eventually, as the Hf concentration is depleted and the oxygen potential is increased locally at these penetrations,  $\text{Al}_2\text{O}_3$  can form and grow by rapid interfacial diffusion, ultimately embedding the initial  $\text{HfO}_2$  precipitates [63]. The process is preferred at the Hf-rich areas, such as coating grain boundaries.

While pegging is currently considered a non-causative artifact regarding reactive element effects on scale adhesion, the sulfur content remains to be a critical factor. Briefly, it has been shown repeatedly that ppm levels of sulfur in the bulk can segregate to high levels at the metal surface or oxide-metal interface at high temperature. Reactive element additions prevent deleterious effects on scale adhesion, in large part by reducing the sulfur activity in the alloy and reducing segregation. Pt is also very effective in counteracting the sulfur effects, however the possible mechanism(s) must be substantially different [11, 12]. In any event, the substrate, baseline and Hf-doped coatings exhibit considerable sulfur contents, 30, 250, and 110 ppmw, respectively. Sulfur from both sources may have thus played a major role in deteriorating the cyclic oxidation performance of these samples. While it is known that sulfur impurities enter aluminide coatings in CVD processing [64], the substrate amount could be reduced by using low sulfur ( $<1$  ppmw), second generation single crystal superalloys. These substrates, with their higher aluminum contents, should lead to improved cyclic oxidation behavior.

The surface structures presented some familiar and unusual features. In the cited studies of aluminized superalloys, a network of alumina scale ridges was common during protective growth and was the site of fine  $\text{HfO}_2$  precipitates for those systems with Hf. Such a network was not observed here, possibly due to the fine structure of the coatings and

the domination of coating grain boundary and cusp-like features. Regarding degraded structures, comparison to some details from an 1150°C, 2000 h cyclic test of Ni(Pt)Al coated CMSX4 may apply, particularly regarding secondary oxide formations [65]. In one protective sample, the alumina scale grain boundary ridges were decorated with a fine, uniform distribution of monoclinic (Hf,Ti)O<sub>2</sub> particles. But another sample produced steady state weight losses and exhibited interfacial spallation. Crystallographically faceted (Ni,Co)(Al,Cr)<sub>2</sub>O<sub>4</sub> spinel, with an α-Al<sub>2</sub>O<sub>3</sub> base scale were the dominant features. Other regions exhibited nodular spinel grains, with fine (Ta,Ti)-rich rutile particles decorating the spinel. The spinel regions were regarded as re-oxidized areas that had previously spalled to bare metal, exposing a surface with insufficient Al content to re-form alumina. Many of these features are represented in the present study.

The cross-sections clearly demonstrated Al depletion due to the formation of Al<sub>2</sub>O<sub>3</sub> scales and interdiffusion with the substrate. By contrast, in bulk NiAl cast alloys [13, 41, 66, 25-31], Al depletion due to interdiffusion is absent. Doped cast alloys also possess a more uniform Hf distribution. Consequently, greater cyclic oxidation lifetimes are expected on Hf-doped NiAl cast alloys than on Hf-modified NiAl coatings.

Finally, Hf additions decreased the surface rumpling during oxidation compared to both NiAl and Pt-NiAl coatings. Similar results have been observed during 1150°C oxidation testing of a Ni(Pt)Al aluminide coatings on Ni-base substrates with different Hf contents [40]. Although there are many coupled origins of the rumpling phenomenon [66-68], it is generally agreed that reducing rumpling of the coating can increase the creep strength significantly. The improved creep strength of Hf-doped bulk NiAl has been well documented [70-71]. Decreased bond coat rumpling is expected to increase the adherence of the ceramic top coat and so improve the lifetime of TBC systems in engine service environments [18, 19], as recently demonstrated commercially [49,50].

## 5. SUMMARY

Simple β-NiAl, Hf-modified β-NiAl, Pt-diffused, Pt-modified β-(Ni,Pt)Al+ξ-(PtAl<sub>2</sub>), and Hf-modified β-(Ni,Pt)Al coatings were produced on Inconel-718 substrates and tested in cyclic 1050°C oxidation in air up to 4370h, showing:

- (1) Hf additions to both simple aluminide and Pt-modified aluminide coatings improved the adherence of oxide scales, reduced rumpling, and extended the coating lifetime.
- (2) Both Hf-doped coatings formed an outer surface network of Hf-rich ridges at the coating grain boundaries that oxidized to dispersed HfO<sub>2</sub> particles; Hf-rich areas also oxidized to HfO<sub>2</sub> particles embedded within the α-Al<sub>2</sub>O<sub>3</sub> scales and as intrusions in the metal (pegs).

- (3) Pt-doping was very effective in improving the cyclic oxidation behavior in both the Pt-NiAl and Hf-Pt-NiAl coatings.
- (4) Optimum adhesion and growth behavior may not have been demonstrated because of high initial sulfur and low aluminum contents in the alloy, over-doping with Hf resulting in excess HfO<sub>2</sub> formation, and secondary effects due to substrate Fe, Ti, Nb diffusion into the coating.
- (5) Diffused Pt coatings without aluminizing did not exhibit any noticeable oxidation protection due to the low Al content of the Inconel 718 substrate and intrinsic inability to form alumina scales.

## ACKNOWLEDGEMENTS

This work is a part of SIFCO Hf-modified aluminide coating research and development program with a goal to investigate the beneficial effects of Hf additions during 2008-2011. Program management support by Jeff Thrun, Mike Christopher, Tom Anderson, Jerry Oss, Dan Lindau; vapor phase coating process and heat treatment support by Guy Sayre; metallurgical sample preparation by Randy Watkins; SEM/EDS analysis by Dieter Scholz at Materials Engineering and Evaluation; GDMS analysis by Karol Putyera at Evans Analytical Group; and XRD analysis of surface scales by Richard B. Rogers of NASA GRC are gratefully acknowledged.

## REFERENCES

- [1] Hindam H, Whittle DP. Microstructure, adhesion and growth kinetics of protective scales on metals and alloys. *Oxid Met* 1982; 18 (5-6): 245-284.  
<http://dx.doi.org/10.1007/BF00656571>
- [2] Miller RA. Oxidation-based model for thermal barrier coating life. *J Am Ceram Soc* 1984; 67 (8) 517-521.  
<http://dx.doi.org/10.1111/j.1151-2916.1984.tb19162.x>
- [3] DeMasi-Marcin JT, Sheffler KD, Bose S. Mechanisms of degradation and failure in a plasma-deposited thermal barrier coating. *J Eng Gas Turbine Power* 1990; 112 (4): 521-526.  
<http://dx.doi.org/10.1115/1.2906198>
- [4] Cocking JL, Richards PG, Johnston GR. Comparative durability of six coating systems on first-stage gas turbine blades in the engines of a long-range maritime patrol aircraft. *Surf Coat Technol* 1988; 36:37-47.  
[http://dx.doi.org/10.1016/0257-8972\(88\)90134-X](http://dx.doi.org/10.1016/0257-8972(88)90134-X)
- [5] Krishna GR, Das DK, Singh V, Joshi SV. Role of Pt content in the microstructural development and oxidation performance of Pt-aluminide coatings produced using a high-activity aluminizing process. *Mater Sci Eng A* 1988; 251: 40-47.  
[http://dx.doi.org/10.1016/S0921-5093\(98\)00655-8](http://dx.doi.org/10.1016/S0921-5093(98)00655-8)
- [6] Fisher G, Chan WY, Datta PK, Burnell-Gray JS. Noble metal aluminide coatings for gas turbines. *Platinum Met Rev* 1999; 43(2): 59-61.
- [7] Zhang Y, Haynes JA, Lee WY, Wright IG, Pint BA, Cooley KM, Liaw PK. Effects of Pt incorporation on the isothermal oxidation behavior of chemical vapor deposition aluminide coatings. *Metall Mater Trans A* 2001; 32: 1727-1741.  
<http://dx.doi.org/10.1007/s11661-001-0150-6>
- [8] Haynes JA, Pint BA, Zhang Y, Wright IG. The effect of Pt content on γ-γ' NiPtAl coatings. *Surf Coat Technol* 2008; 203 (5-7): 413-416.  
<http://dx.doi.org/10.1016/j.surfcoat.2008.08.063>
- [9] Reed RC, Wu RT, Hook MS, Rae CMF, Wing RG. On oxidation behaviour of platinum aluminide coated nickel based superalloy CMSX-4. *Mater Sci Technol* 2009; 25 (2): 276-286.  
<http://dx.doi.org/10.1179/174328408X361481>

- [10] Warnes BM, Punola DC. Clean diffusion coatings by chemical vapor deposition. *Surf Coat Technol* 1997; 94-95: 1-6. [http://dx.doi.org/10.1016/S0257-8972\(97\)00467-2](http://dx.doi.org/10.1016/S0257-8972(97)00467-2)
- [11] Hou PY. Segregation phenomena at thermally grown  $\text{Al}_2\text{O}_3$ /alloy interfaces. *Annu Rev Mater Res* 2008; 38: 275-298. <http://dx.doi.org/10.1146/annurev.matsci.38.060407.130323>
- [12] Gheno T, Monceau D, Oquab D, Cadoret Y. Characterization of sulfur distribution in Ni-based superalloy and thermal barrier coatings after high temperature oxidation: A SIMS analysis. *Oxid Met* 2010; 73 (1-2): 95-113. <http://dx.doi.org/10.1007/s11085-009-9164-z>
- [13] Gleeson B, Wang W, Hayashi S, Sordelet D. Effects of platinum on the interdiffusion and oxidation behavior of Ni-Al-based alloys. *Mater Sci Forum* 2004; 461-464: 213-222. <http://dx.doi.org/10.4028/www.scientific.net/MSF.461-464.213>
- [14] Copland E. Thermodynamic effect of platinum addition to  $\beta$ -NiAl: An initial investigation. NASA/CR-2005-213330, NASA, Cleveland, OH, 2005, pp1-28.
- [15] Gleeson B, Mu N, Hayashi S. Compositional factors affecting the establishment and maintenance of  $\text{Al}_2\text{O}_3$  scales on Ni-Al-Pt systems. *J Mater Sci* 2009; 44 (7): 1704-1710. <http://dx.doi.org/10.1007/s10853-009-3251-z>
- [16] Zhang Y, Haynes JA, Pint BA, Wright IG, Lee WY. Martensitic transformation in CVD NiAl and (Ni,Pt)Al bond coatings, *Surf Coat Technol* 2003; 163 -164: 19-24.
- [17] Chen MW, Ott RT, Hufnagel TC, Wright PK, Hemker KJ. Microstructural evolution of platinum modified nickel aluminide bond coat during thermal cycling. *Surf Coat Technol* 2003; 163 -164: 25-30.
- [18] Tolpygo VK, Clarke DR. Surface rumpling of a (Ni,Pt)Al bond coat induced by cyclic oxidation. *Acta Mater* 2000; 48: 3283-3293. [http://dx.doi.org/10.1016/S1359-6454\(00\)00156-7](http://dx.doi.org/10.1016/S1359-6454(00)00156-7)
- [19] Mumm DR, Evans AG, Spitsberg IT. Characterization of a cyclic displacement instability for a thermally growth oxide in a thermal barrier system. *Acta Mater* 2001; 49: 2329-2340. [http://dx.doi.org/10.1016/S1359-6454\(01\)00071-4](http://dx.doi.org/10.1016/S1359-6454(01)00071-4)
- [20] Stringer J, Allam M, Whittle DP. The high temperature oxidation of Co-Cr-Al alloys containing yttrium or hafnium additions. *Thin Solid Films* 1977; 45:377-384. [http://dx.doi.org/10.1016/0040-6090\(77\)90273-5](http://dx.doi.org/10.1016/0040-6090(77)90273-5)
- [21] Allam IM, Whittle DP, Stringer J. The oxidation behavior of CoCrAl systems containing active element additions. *Oxid Met* 1978; 12 (1) 35-66. <http://dx.doi.org/10.1007/BF00609974>
- [22] Allam IM, Whittle DP, Stringer J. Improvements in oxidation resistance by dispersed oxide addition:  $\text{Al}_2\text{O}_3$ -forming alloys. *Oxid Met* 1979; 13 (4) 381-401. <http://dx.doi.org/10.1007/BF00609306>
- [23] Pendse R, Stringer J. The influence of alloy microstructure on the oxide morphology in a Co-10% Cr-11%Al alloy with and without reactive element additions. *Oxid Met* 1985; 23 (1-2): 1-16. <http://dx.doi.org/10.1007/BF01095804>
- [24] Khanna AS, Wasserfuhr C, Quadackers WJ, Nickel H. Addition of yttrium, cerium and hafnium to combat the deleterious effect of sulphur impurity during oxidation of a Ni-Cr-Al alloy. *Mater Sci Eng A* 1989; 120: 185-191. [http://dx.doi.org/10.1016/0921-5093\(89\)90738-7](http://dx.doi.org/10.1016/0921-5093(89)90738-7)
- [25] Pint PA, Wright IG, Lee WY, Zhang Y, Průšner K, Alexander KB. Substrate and bond coat compositions: factors affecting alumina scale adhesion. *Mater Sci Eng A* 1998; 245: 201-211. [http://dx.doi.org/10.1016/S0921-5093\(97\)00851-4](http://dx.doi.org/10.1016/S0921-5093(97)00851-4)
- [26] Pint BA, Haynes JA, More KL, Wright IG, Leyens C. Compositional effects on aluminide oxidation performance: objectives for improved bond coats. In: Pollock TM, Kissinger RD, Bowman RR, Green KA, McLean M, Olson S, Schirra JJ, editors. *Superalloys 2000*, TMS (7th Minerals, Metals & Materials Society); 2000: p. 629-638.
- [27] Leyens C, Pint BA, Wright IG. Effect of composition on the oxidation and hot corrosion resistance of NiAl doped with precious metals. *Surf Coat Technol* 2000; 133-134: 15-22. [http://dx.doi.org/10.1016/S0257-8972\(00\)00878-1](http://dx.doi.org/10.1016/S0257-8972(00)00878-1)
- [28] Haynes JA, Pint PA, More KL, Zhang Y, Wright IG. Influence of sulfur, platinum, and hafnium on the oxidation behavior of CVD NiAl bond coatings. *Oxid Met* 2002; 58 (5-6): 513-544. <http://dx.doi.org/10.1023/A:1020525123056>
- [29] Pint BA, More KL, Wright IG. Effect of quaternary additions on the oxidation behavior of Hf-doped NiAl. *Oxid Met* 2003; 59 (3-4): 257-283. <http://dx.doi.org/10.1023/A:1023087926788>
- [30] Pint BA. The role of chemical composition on the oxidation performance of aluminide coatings. *Surf Coat Technol* 2004; 188-189: 71-78. <http://dx.doi.org/10.1016/j.surfcoat.2004.08.007>
- [31] Pint BA, Haynes JA, Besmann TM. Effect of Hf and Y alloy additions on aluminide coating performance. *Surf Coat Technol* 2010; 204: 3287-3293. <http://dx.doi.org/10.1016/j.surfcoat.2010.03.040>
- [32] Izumi T, Mu N, Zhang L, Gleeson B. Effects of targeted  $\gamma$ -Ni+ $\gamma$ '-Ni3Al-based coating compositions on oxidation behavior. *Surf Coat Technol* 2007; 202: 628-631. <http://dx.doi.org/10.1016/j.surfcoat.2007.08.014>
- [33] Pint BA. Optimization of reactive-element additions to improve oxidation performance of alumina-forming alloys. *J Am Ceram Soc* 2003; 86 (4): 686-695. <http://dx.doi.org/10.1111/j.1151-2916.2003.tb03358.x>
- [34] Pint BA, Schneibel JH. The effect of carbon and reactive element dopants on oxidation lifetime of FeAl. *Scripta Mater* 2005; 52:1199-1204. <http://dx.doi.org/10.1016/j.scriptamat.2005.03.008>
- [35] Gupta DK, Duvall DS. A silicon and hafnium modified plasma sprayed MCrAlY coating for single crystal superalloys. In: Gell M, Kortovich CS, Bricknell RH, Kent WB, Radavich JF, editors. *Superalloys 1984*, TMS, Warrendale, PA;1984: p. 711-720. [http://dx.doi.org/10.7449/1984/Superalloys\\_1984\\_711\\_720](http://dx.doi.org/10.7449/1984/Superalloys_1984_711_720)
- [36] Whittle DP, Stringer J. Improvement in properties: additives in oxidation resistance. *Phil. Trans. R. Soc. Lond. A* 1980; 295: 309-329. <http://dx.doi.org/10.1098/rsta.1980.0124>
- [37] Meier GH. Research on oxidation and embrittlement of intermetallic compounds in the U.S. *Mater Corros* 1996; 47: 595-618.
- [38] Stringer J. The reactive element effect in high-temperature corrosion. *Mater Sci Eng A* 1989; 120-121: 129-137. [http://dx.doi.org/10.1016/0921-5093\(89\)90730-2](http://dx.doi.org/10.1016/0921-5093(89)90730-2)
- [39] Pint BA. Experimental observations in support of the dynamic-segregation theory to explain the reactive-element effect. *Oxid Met* 1996; 45 (1-2): 1-37. <http://dx.doi.org/10.1007/BF01046818>
- [40] Smialek JL, Lowell CE. Effects of diffusion on aluminum depletion and degradation of NiAl coatings. *J Electrochem Soc* 1974; 121 (6): 800-805. <http://dx.doi.org/10.1149/1.2401922>
- [41] Zhang Y, Stacy JP, Pint BA, Haynes JA, Hazel BT, Nagaraj BA. Interdiffusion behavior of Pt-diffused  $\gamma$ + $\gamma'$  coatings on Ni-based superalloys. *Surf Coat Technol* 2008; 203: 417-421. <http://dx.doi.org/10.1016/j.surfcoat.2008.08.053>
- [42] Tolpygo VK, Murphy KS, Clarke DR. Effect of Hf, Y and C in the underlying superalloy on the rumpling of diffusion aluminide coatings. *Acta Mater* 2008; 56: 489-499. <http://dx.doi.org/10.1016/j.actamat.2007.10.006>
- [43] Muamba JMN, Streiff R, Boone DH. L'Influence du Hafnium du Substrat sur la Résistance à l'Oxydation des Revêtements d'Aluminures sur les Superalloys Base Nickel\* (oxidation of Hf modified substrate). *Mater Sci Eng* 1987; 88: 111-121. [http://dx.doi.org/10.1016/0025-5416\(87\)90074-7](http://dx.doi.org/10.1016/0025-5416(87)90074-7)
- [44] Streiff R, Muamba JMN. Mechanisms of the hafnium effect in high-temperature oxidation of aluminide coatings. *JOM* 1988; 40 (11): 104.
- [45] Warnes BM. Reactive element modified chemical vapor deposition low activity platinum aluminide coatings. *Surf Coat Technol* 2001; 146-147: 7-12. [http://dx.doi.org/10.1016/S0257-8972\(01\)01363-9](http://dx.doi.org/10.1016/S0257-8972(01)01363-9)
- [46] Kim GY, He LM, Meyer JD, Quintero A, Haynes JA, Lee WY. Mechanisms of Hf dopant incorporation during the early stage of chemical vapor deposition aluminide coating growth under continuous doping conditions. *Metall Mater Trans A* 2004; 35:3581-3593. <http://dx.doi.org/10.1007/s11661-004-0194-5>
- [47] Haynes JA, Zhang Y, Cooley KM, Walker L, Reeves KS, Pint BA. High-temperature diffusion barriers for protective coatings. *Surf Coat Technol* 2004; 188-189: 153-157. <http://dx.doi.org/10.1016/j.surfcoat.2004.08.066>
- [48] Ford S, Kartono R, Young R. Oxidation resistance of Pt-modified  $\gamma/\gamma'$  Ni-Al at 1150 °C. *Surf Coat Technol* 2010; 204: 2051-2054. <http://dx.doi.org/10.1016/j.surfcoat.2009.08.027>
- [49] Murphy KS, inventor; Howmet Corporation, assignee. Pt-Al-Hf/Zr Coating and Method. U.S. Patent Application, 2010/0297471 A1, Nov. 25, 2010.
- [50] Hazel B, Rigney J, Gorman M, Boutwell B, Darolia R. Development of improved bond coat for enhanced turbine durability. In: Reed RC,

- Green KA, Caron P, Gabb TP, Fahrman MG, Huron ES, Woodard SA, editors. *Superalloys 2008*, TMS, Champion, PA; 2008: p.753-760. [http://dx.doi.org/10.7449/2008/Superalloys\\_2008\\_753\\_760](http://dx.doi.org/10.7449/2008/Superalloys_2008_753_760)
- [51] Wang YQ, Suneson M, Sayre G. Synthesis of Hf-modified aluminide coatings on Ni-base superalloys. *Surf Coat Technol* 2011; 206: 1218-1228. <http://dx.doi.org/10.1016/j.surfcoat.2011.08.031>
- [52] Wang YQ, Sayre G. Factors affecting the microstructure of platinum-modified aluminide coatings during a vapor phase aluminizing process. *Surf Coat Technol* 2009; 203: 1264-1272. <http://dx.doi.org/10.1016/j.surfcoat.2008.10.031>
- [53] Zhang Y, Wang YQ. Effect of Hf additions on aluminide coatings and oxidation performance, unpublished research experimental data – partial data were included in Wang YQ's Ph.D. Dissertation, 2006.
- [54] Smialek JL. Effect of sulfur removal on Al<sub>2</sub>O<sub>3</sub> scale adhesion. *Metall Trans A* 1991; 22: 739-752. <http://dx.doi.org/10.1007/BF02670297>
- [55] Meier GH, Pettit FS, Smialek JL. The effects of reactive element additions and sulfur removal on the adherence of alumina to Ni- and Fe-base alloys. *Mater Corros* 1995; 46: 232-240. <http://dx.doi.org/10.1002/maco.19950460407>
- [56] Pieraggi B. Calculations of parabolic reaction rate constants. *Oxid Met* 1987; 27 (3-4): 177-185. <http://dx.doi.org/10.1007/BF00667057>
- [57] Rybicki GC, Smialek JL. Effect of the  $\theta$ - $\alpha$ -Al<sub>2</sub>O<sub>3</sub> transformation on the oxidation behavior of  $\beta$ -NiAl + Zr. *Oxid Met* 1989; 31 (3-4): 275-304. <http://dx.doi.org/10.1007/BF00846690>
- [58] Graham HC, Davis HH. Oxidation/vaporization kinetics of Cr<sub>2</sub>O<sub>3</sub>. *J Am Ceram Soc* 1971; 54: 89-93. <http://dx.doi.org/10.1111/j.1151-2916.1971.tb12225.x>
- [59] Tedmon CS, Jr. The effect of oxide volatilization on the oxidation kinetics of Cr and Fe-Cr alloys. *J Electrochem Soc* 1966; 113 (8): 766-768. <http://dx.doi.org/10.1149/1.2424115>
- [60] Pint BA. Progress in understanding the reactive element effect since the Whittle and Stringer literature review. In: Tortorelli PF, Wright IG, Hou PY, editors. *Proc. John Stringer Symposium on High Temperature Corrosion*. ASM International, Materials Park, OH, 2003:p. 9–19.
- [61] Ribaudo C, Sircar S, Mazumder J. Laser-clad Ni70Al20Cr7Hf3 alloys with extended solid solution of Hf: Part II. Oxidation behavior. *Metall Mater Trans A* 1989; 20: 2489-2497. <http://dx.doi.org/10.1007/BF02666684>
- [62] Grabke HJ. Segregation and oxidation. *Materiali In Tehnologije* 2006;40: 39-47.
- [63] Hindam H, Whittle DP. Peg formation by short-circuit diffusion in Al<sub>2</sub>O<sub>3</sub> scales containing oxide dispersions. *J Electrochem Soc* 1982; 129 (5): 1147-1149. <http://dx.doi.org/10.1149/1.2124044>
- [64] Lee WY, Zhang Y, Wright IG, Pint BA, Liaw PK. Effects of sulfur impurity on the scale adhesion behavior of a desulfurized Ni-based superalloy aluminized by chemical vapor deposition. *Metall Mater Trans A* 1998; 29: 833-841. <http://dx.doi.org/10.1007/s11661-998-0274-z>
- [65] Mialek JL, Garg A. A compendium of scale surface microstructures: Ni(Pt)Al coatings oxidized at 1150°C for 2000 1-hr cycles. NASA/TM—2010-216091, NASA, Washington, D.C., Feb.5, 2010.
- [66] Göbel M, Rahmel A, Schütze M. The isothermal-oxidation behavior of several nickel-base single-crystal superalloys with and without coatings. *Oxid Met* 1993; 39 (3-4): 231-261. <http://dx.doi.org/10.1007/BF00665614>
- [67] Tolpygo VK, Clarke DR. On the rumpling mechanism in nickel-aluminide coatings Part I: an experimental assessment. *Acta Mater* 2004; 52: 5115-5127. <http://dx.doi.org/10.1016/j.actamat.2004.07.023>
- [68] Tolpygo VK, Clarke DR. On the rumpling mechanism in nickel-aluminide coatings Part II: characterization of surface undulations and bond coat swelling. *Acta Mater* 2004; 52: 5129-5141. <http://dx.doi.org/10.1016/j.actamat.2004.07.023>
- [69] Tolpygo VK, Clarke DR. Rumpling of CVD (Ni,Pt)Al diffusion coatings under intermediate temperature cycling. *Surf Coat Technol* 2009; 203: 3278-3285. <http://dx.doi.org/10.1016/j.surfcoat.2009.04.016>
- [70] Locci IE, Dickerson R, Bowman R, Whittenberger JD, Nathal MV, Darolia R. Microstructure and mechanical properties of cast, homogenized and aged NiAl single crystal containing Hf. In Baker I, Darolia R, Whittenberger JD, Yoo MH, editors. *High-Temperature Ordered Intermetallic Alloys V*; Mater. Res. Soc. Symp. Proc. 288; Pittsburgh, PA 1993; 288: 685-690.
- [71] Noebe R, Bowman R. Review of the physical and mechanical properties and potential applications of the compound NiAl. *International Mater Rev* 1993; 38: 193-232. <http://dx.doi.org/10.1179/imr.1993.38.4.193>

© 2014 Wang *et al.*; Licensee Lifescience Global.

This is an open access article licensed under the terms of the Creative Commons Attribution Non-Commercial License (<http://creativecommons.org/licenses/by-nc/3.0/>) which permits unrestricted, non-commercial use, distribution and reproduction in any medium, provided the work is properly cited.